GEORG-AUGUST-UNIVERSITÄT
GÖTTINGEN

Fakultät für
Physik

Bachelor's Thesis

Machbarkeitsstudien zur direkten Messung der Zerfallsbreite des Top-Quarks

Feasibility Studies of Direct Measurements of the Top Quark Decay Width

prepared by

Knut Zoch

from Wittmund

at the II. Institute of Physics

Thesis number:	II.Physik-UniGö-BSc-2014/01
Thesis period:	21st October 2013 until 27th January 2014
Supervisor:	Priv.-Doz. Dr. Kevin Kröninger
First referee:	Prof. Dr. Arnulf Quadt
Second referee:	Prof. Dr. Ariane Frey

Abstract

In this thesis, the measurability of the top-quark decay width Γ_t is examined. Feasibility studies are done to pursue the question if it is possible to directly measure Γ_t at the LHC with high precision. For this, simplified models are created in which the real situation of a measurement of Γ_t is simulated by using pseudo-data samples. Furthermore, sensitivity studies are presented to test to what extent the different physical and model-based parameters affect the results.

The studies yield that the decay width of the top quark Γ_t will be measurable precisely with the full data sets of the $\sqrt{s} = 7\,\text{TeV}$ and $8\,\text{TeV}$ runs at the LHC. The results are heavily affected by the binning of the pseudo-data samples as well as by the amount of data that is used for the decay-width reconstruction. The detector resolution, which is implemented in the model in form of a Gaussian distribution, also has a great influence on the results. Especially a good knowledge of the resolution distribution, i.e. a small uncertainty on its parameters, leads to a more precise determination of the decay width.

Zusammenfassung

In dieser Arbeit wird die Messbarkeit der Zerfallsbreite des Top-Quarks Γ_t untersucht. Es werden Machbarkeitsstudien vorgestellt, in denen der Frage nachgegangen wird, ob eine direkte Messung von Γ_t am LHC mit hoher Präzision möglich ist. Hierfür werden stark vereinfachte Modelle genutzt, in denen die reale Situation einer Messung von Γ_t mithilfe von Pseudo-Datensätzen simuliert wird. Des Weiteren werden Sensitivitätsstudien präsentiert, in denen ausgetestet wird, inwieweit die verschiedenen physikalischen Parameter und Modellparameter Einfluss auf die Resultate haben.

Die Studien ergeben, dass die Zerfallsbreite des Top-Quarks Γ_t mit hoher Präzision am LHC messbar sein wird, wenn man die kompletten Datensätze der Schwerpunktsenergien $\sqrt{s} = 7\,\text{TeV}$ und $8\,\text{TeV}$ berücksichtigt. Die Resultate werden dabei stark vom Binning der Pseudo-Datensätze und von der Datenmenge, die für die Rekonstruktion benutzt wird, beeinflusst. Die Detektor-Auflösung, die in dem Modell in Form einer Gaußverteilung implementiert ist, hat ebenfalls großen Einfluss auf die Ergebnisse. Besonders eine gute Kenntnis der Auflösungsfunktion (also eine geringe Unsicherheit auf ihre Parameter) führt zu präziseren Ergebnissen in der Bestimmung der Zerfallsbreite.

Contents

1. Introduction

One of the most prominent branches of physics is the area of elementary particle physics. Over the last years, the subject has become popular especially because of a large presence in the media: the construction of the Large Hadron Collider (LHC) at CERN (Geneva), which was commissioned in 2010; the discovery of a boson consistent with the long-sought Higgs boson by the LHC collaborations ATLAS and CMS in 2012 [1, 2]—followed by the awarding of the Nobel Prize in Physics to Peter Higgs and François Englert who had already postulated its existence in 1964 [3, 4].

However, particle physics is one of the youngest areas of physics which has only developed in the course of the last century. The most popular model of elementary particle physics—the Standard Model—was established only about forty years ago although the idea that matter is made of small indivisible particles originates from the ancient Greeks. Since the 90s it is possible to produce such high energies that even the heaviest particle known today, the top quark, is produced. The top quark was discovered in 1995 by the CDF and DØ collaborations at the TEVATRON collider at FERMILAB (Chicago) [5, 6]. The "jigsaw puzzle" of elementary particles was finally pieced together with the possible discovery of the Higgs boson last year that had been (according to current knowledge) the last missing particle.

While the time of scrutinizing the Higgs boson has just begun, most of the properties of the top quark have already been determined at the TEVATRON. But only since the commissioning of the LHC, it is possible to produce heavy particles like the top quark in large numbers so that statistical uncertainties can be reduced significantly. With such high statistics, physicists hope to gain more accurate knowledge about so far only inaccurately determined parameters of the top quark.

The following feasibility studies deal with one of these parameters, the decay width of the top quark, for which only rough measurements have been made until today. This thesis pursues the question if it is possible to directly measure the top-quark decay width at the LHC—under the condition that all other parameters (e.g. the technical parameters of the used particle detector) are known with sufficient accuracy. At first, the underlying theoretical and experimental principles are summarized. This is followed by a brief

discussion of the problems encountered in the measurement of the decay width. Then simple models are presented to test the measurability of the decay width imitating the real situation by the use of pseudo-data samples. In addition, studies of the influence of other parameters on this measurability are conducted in the form of sensitivity studies.

2. Theoretical Foundation

The entire field of modern elementary particle physics is based on a model called the Standard Model of particle physics (SM). It comprises all the currently known elementary particles: twelve fermions, four kinds of gauge bosons mediating the interactions, and the Higgs boson (see figure 2.1). While for example the photon γ is its own anti-particle, there are specific anti-particles for each fermion and the W bosons with identical properties except for the charge-like properties (e.g. electric charge) which are of opposite sign. The SM, which is mathematically described by a gauge-quantum-field theory, is represented by the unitary product group $SU(3)_C \times SU(2)_L \times U(1)_Y$.

In the following section, a brief introduction to the particles and forces of the SM is given; this is followed by a more precise theoretical description of the weak interaction. In the last part, there is a short summary of the physics of the top quark. Because the following theory is part of every particle-physics textbook, this section is kept short. Unless stated otherwise, all information is taken from Griffiths [7].

2.1. The Standard Model of Particle Physics

The fermions of the SM are described in terms of two of their properties: the electric charge[1] Q and the third component of the weak isospin T, denoted as T_3. Both properties are combined to the weak hypercharge $Y_W = 2(Q - T_3)$ similar to the concept of strong hypercharge described by the Gell-Mann–Nishijima formula [10, 11]. The twelve fermions of the SM are further divided into two groups of particles: quarks and leptons.

The quarks consist of six different types of particles known as flavours: up (u), down (d), charm (c), strange (s), top (t), and bottom (b). They are summarized in three generations each consisting of two quarks as shown in the following table.

	1st gen.	2nd gen.	3rd gen.
up-type	u	c	t
down-type	d	s	b

[1] Q is denoted in units of the elementary charge $e \approx 1.602 \cdot 10^{-19}$ C [9].

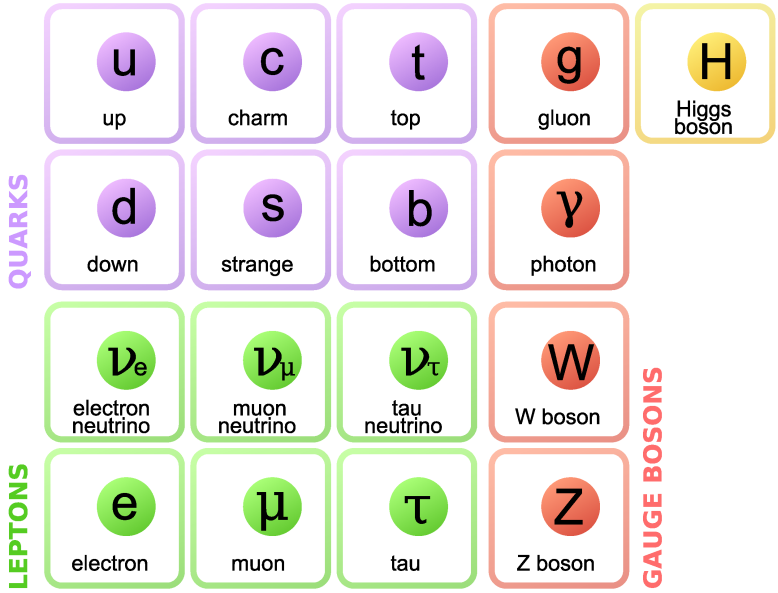

Figure 2.1.: The particles and bosons known today (modified version of [8]).

The upper of the two quarks carries an electric charge of $Q = {}^{+2}/_{3}$ and is called up-type quark according to the respective quark of the first generation. The remaining three are called down-type quarks and carry $Q = {}^{-1}/_{3}$. The existence of the quarks was proposed only in 1964 [12, 13] because they do not exist—in contrast to leptons—as single particles in nature due to an effect called confinement[2]. Free quarks hadronize: along with other quarks they form compound particles called hadrons (e.g. protons and neutrons).

Due to their different coupling behaviour in the weak interaction, they are further differentiated in terms of their helicity, i.e. one further distinguishes between left- and right-handed particles. Therefore, quarks are formally divided into three doublets of left-handed quarks, where the upper quarks carry $I_3 = {}^{+1}/_{2}$ and the lower $I_3 = {}^{-1}/_{2}$, and six right-handed quark singlets with $I_3 = 0$:

$$\begin{aligned} Q_L^i &= \begin{pmatrix} u \\ d \end{pmatrix}_L, & \begin{pmatrix} c \\ s \end{pmatrix}_L, & \begin{pmatrix} t \\ b \end{pmatrix}_L \\ u_R^i &= u_R, & c_R, & t_R \\ d_R^i &= d_R, & s_R, & b_R \end{aligned} \tag{2.1}$$

Leptons are categorized in a similar way. There are three generations as well where each of them contains a charged particle with $Q = -1$ and an uncharged neutrino. The first generation comprises the electronic leptons which includes the electron e^- and the electron

[2]The confinement is caused by the strong interaction (and therefore exists only for colour-charged particles): the strong force between two quarks is weaker for shorter distances than for longer.

neutrino ν_e. The second generation, called muonic leptons, and the third generation, called tauonic leptons, contain the muon μ^- and the muon neutrino ν_μ, and the tau τ^- and the tau neutrino ν_τ, respectively. They are also divided into left- and right-handed leptons: While the left-handed leptons are summarized in doublets as well (with the upper and lower particle carrying $I_3 = {}^{+1}/_2$ and $I_3 = {}^{-1}/_2$, respectively), right-handed neutrinos are predicted to be non-existent by the SM.[3] Therefore, there are only three right-handed leptons with $I_3 = 0$ which are denoted as singlets:

$$\begin{pmatrix} \nu_e \\ e^- \end{pmatrix}_L , \begin{pmatrix} \nu_\mu \\ \mu^- \end{pmatrix}_L , \begin{pmatrix} \nu_\tau \\ \tau^- \end{pmatrix}_L , \; e_R^-, \; \mu_R^-, \; \tau_R^- \tag{2.2}$$

There are four fundamental interactions acting on the particles: strong, weak, electromagnetic, and gravitational force. They differ in their strength and in the way in which they are mediated. An overview of their most important properties is given in table 2.1. In particle physics, gravity is usually ignored because its effects are only visible on a macroscopic scale.[4] Besides, not all forces act on every type of particles. The electromagnetic interaction acts only on electrically charged particles. The strong interaction is only mediated between particles carrying a colour charge (which is the charge of the strong interaction), i.e. the six quarks and the eight gluons which are the gauge bosons of the strong interaction. The weak interaction comprises charged and neutral currents mediated by the charged $W^\pm$ and the uncharged Z^0 bosons, respectively. While neutral currents act on every fermion of the standard model (and on the gauge bosons as well), charged currents are only mediated between particles with $T_3 \neq 0$, i.e. only left-handed particles and the corresponding right-handed anti-particles.

Force	Strength	Theory	Mediator
Strong	10	QCD	Gluon
Electromagnetic	10^{-2}	QED	Photon
Weak	10^{-13}	QFD	$W^\pm$ and Z^0
Gravitational	10^{-42}	General relativity	?

Table 2.1.: The fundamental forces and their most important properties [7].

[3] The SM predicts that neutrinos are massless particles and therefore propagate with the speed of light. This leads to the statement that there are no right-handed neutrinos because of the extraordinary couplings of the weak interaction (described in more detail in section 2.2). However, there is direct evidence in neutrino-oscillation experiments disproving this prediction [14–16]; although the origin of this phenomenon is not yet understood.

[4] Additionally, gravity differs from the other interactions a lot and cannot be described in the same way: electromagnetic, strong, and weak interaction are all mediated by gauge bosons (e.g. the photon γ mediates the electromagnetic force) while the mediation processes of gravity are not yet understood.

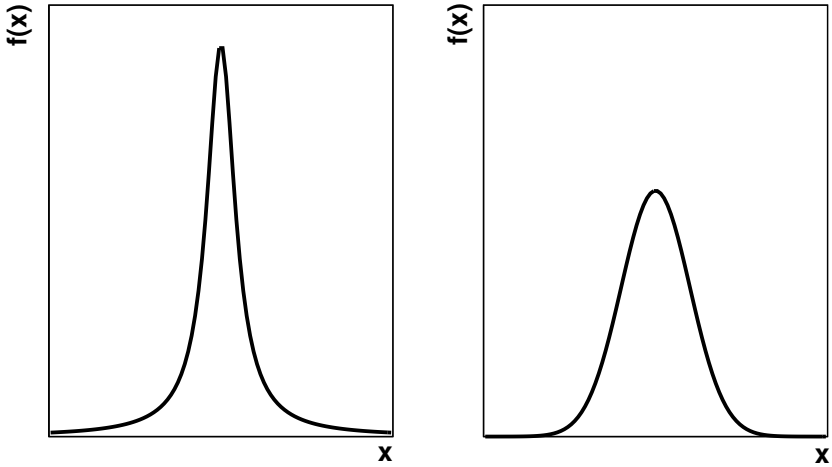

Figure 2.2.: Comparison of a Breit-Wigner distribution (left) with a normal distribution (right); both functions are normalized to the same value.

The recently discovered boson is consistent with the Higgs boson which plays a paramount role in the SM. The corresponding Higgs field, proposed by three groups of physicists in 1964 [3, 4, 17], endows all particles with mass, especially the two massive gauge bosons $W^{\pm}$ and Z^0 of the weak interaction. This acquisition of mass, known as the Higgs mechanism, is described in terms of field theory by spontaneous symmetry breaking without violating gauge theories. With this, a new particle is introduced: the Higgs boson H.

The elementary particles share a common principle: Unless prevented by a conservation law, they tend to decay into lighter particles.[5] Due to its finite lifetime, an unstable particle has a physically-based uncertainty on its mass caused by the Heisenberg uncertainty principle [18]: The mass distribution is not a single δ peak, but a Breit-Wigner distribution with a parameter Γ (called *decay width*) describing the width of the distribution. More precisely, Γ is the full width of the distribution at half maximum (*FWHM*). Figure 2.2 shows the typical profile of a Breit-Wigner distribution compared to a Gaussian (or: normal) distribution. The uncertainty principle $\Delta t \cdot \Delta E \geq 2\hbar$ [19] directly leads to the following relation between the decay width Γ and the lifetime τ of a particle:

$$\Gamma = \frac{\hbar}{\tau} \tag{2.3}$$

where $\hbar = 6.582 \cdot 10^{-16}\,\mathrm{eV\,s}$ is the reduced Planck constant [9] and Γ is identified with $2 \cdot \Delta E$ and τ with Δt. Since the mean lifetime of a particle is very difficult to measure directly, it can therefore be calculated by measuring the width of the mass distribution of an ensemble of particles.

[5] The electron is for example a stable particle, because it is the lightest charged particle and therefore cannot decay to a lighter mass (charge conservation).

2.2. The Weak Interaction

The weak interaction is one of the four fundamental forces of the SM; it is mediated by the massive gauge bosons $W^{\pm}$ and Z^0 with masses of $m_W \approx 80.4\,\text{GeV}$ and $m_Z \approx 91.2\,\text{GeV}$, respectively [9]. Processes involving the W or the Z are often referred to as charged and neutral current processes. As already mentioned, charged currents only interact with particles with $I_3 \neq 0$, i.e. only left-handed quarks and leptons (and their right-handed anti-particles). Consequently, the weak interaction is the only fundamental interaction breaking parity symmetry between particles/anti-particles [20] (or in further consequence even charge-parity symmetry [21]).

Since the W is a charged boson, its coupling to a fermion changes the fermion's charge, i.e. charged leptons are converted to the corresponding uncharged neutrinos and vice versa. In the same way, up-type quarks are converted to the corresponding down-type quarks and the other way around. While the conversion of leptons is limited to the corresponding doublet of the particle as denoted in eq. (2.2), quarks can be converted from one generation to another. To describe the cross-generational transitions, modified quark states, called weak eigenstates, are introduced [22–24]. They are linear combinations of the mass eigenstates and are denoted as follows:

$$\begin{pmatrix} u \\ d' \end{pmatrix}, \begin{pmatrix} c \\ s' \end{pmatrix}, \begin{pmatrix} t \\ b' \end{pmatrix} \qquad \text{where} \quad \begin{pmatrix} d' \\ s' \\ b' \end{pmatrix} = \begin{pmatrix} V_{ud} & V_{us} & V_{ub} \\ V_{cd} & V_{cs} & V_{cb} \\ V_{td} & V_{ts} & V_{tb} \end{pmatrix} \begin{pmatrix} d \\ s \\ b \end{pmatrix} \tag{2.4}$$

The 3×3 matrix $V_{CKM} = \boldsymbol{V}_L^{\,u}\, \boldsymbol{V}_L^{\,d\dagger}$ is called CKM matrix and describes the quark mixing in the weak interaction. If V_{CKM} was the unit matrix, the conversions of quarks would be limited to their generation as well. However, the current experimental values are [9]:

$$V_{CKM} \approx \begin{pmatrix} 0.9743 & 0.2253 & 0.0035 \\ 0.2252 & 0.9734 & 0.0412 \\ 0.0087 & 0.0404 & 0.9991 \end{pmatrix} \tag{2.5}$$

Because of this unique changing of the flavour, the weak interaction is responsible for a lot of particle decays, e.g. the decay of the top quark and the β decay of radioactive nuclei.

In the SM, the weak interaction is unified with the electromagnetic force to the *electroweak* interaction described by a $SU(2)_L \times U(1)_Y$ gauge theory. The group $SU(2)_L$ refers to the weak isospin T (the subscript L means that only left-handed states are involved) and $U(1)_Y$ to the weak hypercharge Y as described in the previous section.

2.3. Top Quark Physics

Forming the third generation of quarks in the SM (along with the bottom quark), the top quark is of special interest because of its unique high mass. Due to technical limitations to achieve such high energies at colliders, physicists failed to discover the top quark for many years, although its existence was already predicted in 1973 by Kobayashi and Maskawa [24]. The discovery was finally made in 1995 by the CDF and DØ collaborations [5, 6]. Since then, its mass has been determined at Fermilab and Cern with high accuracy. The combined results of CDF/DØ (Tevatron) and Atlas/Cms (Lhc) measure the top-quark mass to be [25, 26]:

$$m_t = 173.18 \pm 0.94\,\text{GeV} \quad (\text{CDF/D}\text{Ø}) \tag{2.6a}$$

$$m_t = 173.29 \pm 0.95\,\text{GeV} \quad (\text{Atlas/Cms}) \tag{2.6b}$$

In the following subsection, the top quark's properties are explained in more detail. In particular, its extremely short lifetime is discussed. Afterwards, the production mechanisms of the top quark as well as its decay are described.

2.3.1. Properties of the Top Quark

Since the top quark belongs to the third generation of quarks, it is unstable and therefore decays to lighter particles. Its unique high mass causes exceptionally rapid decays of top quarks with lifetimes far below the measurable time scale.

According to equation (2.3) the mass distribution of top quarks has a certain decay width Γ_t due to the finite lifetime. Since the lifetime is extremely short, the decay width of the top quark is expected to be relatively small compared to its mass and is therefore difficult to measure as well. In addition to a direct measurement, the top-quark decay width can be determined by SM predictions using precisely measured other SM parameters (next-to-leading order (NLO) approximation) [27]:

$$\Gamma_t \overset{(NLO)}{=} \frac{G_F m_t^3}{8\pi\sqrt{2}} \left(1 - \frac{M_W^2}{m_t^2}\right)^2 \left(1 + 2\frac{m_W^2}{m_t^2}\right) \left[1 - \frac{2\alpha_s}{3\pi}\left(\frac{2\pi^2}{3} - \frac{5}{2}\right)\right] \tag{2.7}$$

where G_F is the Fermi constant, m_t the top mass, m_W the W boson mass, and α_s the coupling constant of the strong interaction. Evaluated for a value of $m_t = 173.2\,\text{GeV}$

according to the latest measurements of the mass in eq. (2.6), equation (2.7) yields:

$$\Gamma_t \approx 1.35\,\text{GeV} \tag{2.8}$$

Despite its small value, the DØ collaboration was able to indirectly measure the decay width of the top quark in 2012.[6] They measured Γ_t to be [28]:

$$\Gamma_t = 2.00^{+0.47}_{-0.43}\,\text{GeV} \tag{2.9}$$

The CDF collaboration calculated the following limits for the decay width [29]:

$$\Gamma_t < 6.38\,\text{GeV} \quad \text{at } 95\%\text{ C.L.} \tag{2.10a}$$

$$1.10 < \Gamma_t < 4.05\,\text{GeV} \quad \text{at } 68\%\text{ C.L.} \tag{2.10b}$$

By using eq. (2.3) the lifetime τ_t was calculated as well. The measurement of DØ in eq. (2.7) and a second measurement by the CDF collaboration yield values of [28, 30]:

$$\tau_t = (3.29^{+0.90}_{-0.63}) \cdot 10^{-25}\,\text{s} \quad (\text{DØ}) \tag{2.11a}$$

$$\tau_t = (2.98^{+3.00}_{-1.35}) \cdot 10^{-25}\,\text{s} \quad (\text{CDF}) \tag{2.11b}$$

Therefore, the mean lifetime of the top quark is currently estimated to be below the typical time scale of hadronization processes of about $3 \cdot 10^{-24}\,\text{s}$ [31, 32], i.e. there are in general no bound states of the top quark. Consequently, there are no top-jets produced by a top quark because it decays before hadronization processes start.

In order to enable a direct determination of the decay width from a top quark produced in a collider, the resolution of the reconstructed top-quark mass must be of the same order of magnitude—at least, the technical limitations like the resolution have to be very accurately known. Besides, a precise reconstruction can only be done with large statistics. The sample of top-quark events at the Fermilab has not been large enough to measure Γ_t with a relative uncertainty below 25% yet[7] (see eq. (2.9) and (2.10)), but the Lhc will provide such large statistics. With current centre-of-mass energies of $\sqrt{s} = 7\,\text{TeV}$ (2010-11) and $\sqrt{s} = 8\,\text{TeV}$ (2012) it is hoped that the statistical uncertainties can be reduced significantly in order to make an accurate measurement of the decay width possible.

[6] For the measurement in [28], the single-top cross section and the branching fraction $\mathcal{B}(t \to Wb)$ were used. This method assumed that the coupling leading to (t-channel) single-top production is identical to the coupling in the top-quark decay.

[7] Tevatron, the collider of Fermilab, is shut down since 2012, but the evaluation of the produced data is still on-going. Thus, the Fermilab results on Γ_t could still be improved in the future.

2.3.2. Production of the Top Quark

The mechanism for the production of a top quark depends on the energy provided by the used particle accelerator. At centre-of-mass energies like $\sqrt{s} = 7\,\text{TeV}$ and higher at which the LHC operates, top quarks are most likely produced in pairs of particle and anti-particle (short: $t\bar{t}$ pairs) via the strong interaction.

Because the LHC is a proton-proton collider, only parts of the energy carried by the two colliding protons are released in a collision. This can be explained with the fact that protons are hadrons and therefore compound particles; all partons included in a proton carry a fraction of the total momentum.[8] In a collision, not the protons but the partons interact with each other. Consequently, only their energy is released, not the total centre-of-mass energy. At $\sqrt{s} > 7\,\text{TeV}$ it is most likely that two virtual gluons or two sea quarks interact when it comes to a "collision" between two protons. The production processes are shown in figure 2.3.

Therefore, a much higher centre-of-mass energy than the invariant $t\bar{t}$ mass of about 350 GeV is needed to create a $t\bar{t}$ pair. This is one of the reasons why there will be a significant difference in the amount of produced $t\bar{t}$ events between the TEVATRON with a maximum of $\sqrt{s} = 1.96\,\text{TeV}$ and the LHC with the latest results at $\sqrt{s} = 8\,\text{TeV}$.

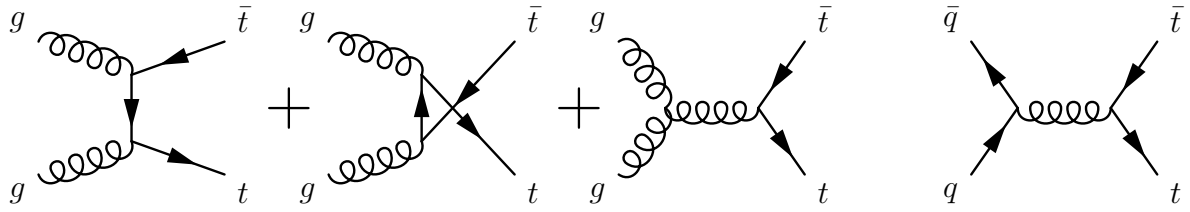

(a) gluon fusion (b) $q\bar{q}$ annihilation

Figure 2.3.: Feynman graphs of $t\bar{t}$ pair production (lowest order).

However, there are possible production mechanisms via the weak interaction leading to a single top quark. They are less likely to occur than pair production, but their existence was confirmed in 2009 by both the CDF and DØ collaborations [33, 34]. The Feynman diagrams showing the possible single-top production processes can be found in figure 2.4. Single-t production is also a subject of current research at the LHC. Although, primarily $t\bar{t}$ production is used to investigate the properties of the top quark because single-t events are much more difficult to distinguish from other processes and are less likely produced.

[8] Protons comprise valence quarks, sea quarks, and gluons. While the valence quarks determine the type of particle (e.g. "up", "up", and "down" means "proton"), the sea quarks and gluons just exist as virtual particles. The distribution of the momentum as a function of the energy is described by the parton distribution functions (PDF).

Looking at the cross sections, there are roughly twice as many pair-production events at a centre-of-mass energy of $\sqrt{s} = 7\,\text{TeV}$. ATLAS measured the single-t cross section and the $t\bar{t}$ cross section to be [35, 36]:

$$\sigma_t = \ 83 \pm \ 4(\text{stat.}) \ {}^{+20}_{-19}(\text{syst.})\,\text{pb} \tag{2.12a}$$

$$\sigma_{t\bar{t}} = 186 \pm 13(\text{stat.}) \pm 20(\text{syst.}) \pm 7(\text{lumi.})\,\text{pb} \tag{2.12b}$$

For comparison, CDF and DØ measure the $t\bar{t}$ cross section at the TEVATRON on the Run II centre-of-mass energy $\sqrt{s} = 1.96\,\text{TeV}$ to be [37]:

$$\sigma_{t\bar{t}} = 7.60 \pm 0.20(\text{stat.}) \pm 0.29(\text{syst.}) \pm 0.21(\text{lumi.})\,\text{pb} \tag{2.13}$$

which is less then one tenth of the estimated LHC cross section.

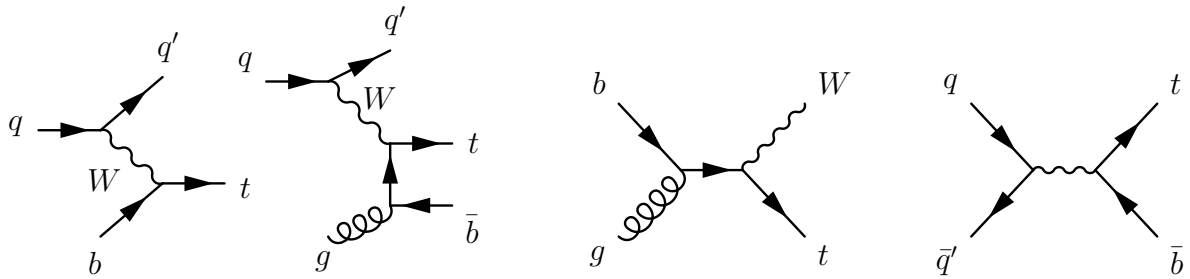

(a) via t-channel (b) tW production (c) via s-channel

Figure 2.4.: Feynman graphs of single top production (lowest order).

2.3.3. The Decay of the Top Quark

The top quark decays almost exclusively into a b quark and W boson via the weak interaction (the branching ratio is often assumed as 100%). The final states Ws and Wd are expected to be suppressed compared to Wb due to the small CKM matrix elements V_{ts} and V_{td} (see eq. (2.5)). While the bottom quark hadronizes immediately and produces a b-quark jet, the W boson has different decay channels. It can either decay leptonically by producing a lepton and its corresponding neutrino or it can decay hadronically by producing an up-type and down-type quark (most likely of the same generation).

Thus, the decay of the top quark can either produce a b-jet and two light jets (originating from the lighter quarks) or a b-jet, a lepton, and a neutrino. $t\bar{t}$ production is therefore subdivided in three different decay channels: the "alljets" channel where both W decay hadronically, the "dilepton" channel where both W decay leptonically, and the "lepton+jets" channel as a mixture of both. Due to the different branching ratios of the

W, which most probably decays hadronically (with a probability of around 68% [9]), the top-quark decay channels have different probabilities, too. They are shown in the pie chart in figure 2.5. On the left-hand side of the figure, a "lepton+jet" decay of a $t\bar{t}$ pair is illustrated.

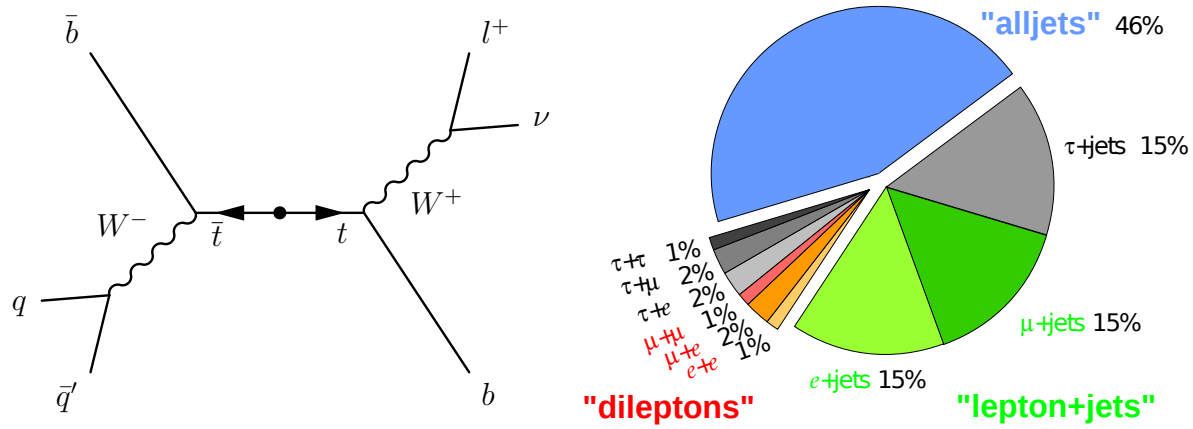

(a) lepton+jets decay of a $t\bar{t}$ pair

(b) Branching fractions for $t\bar{t}$ decays [38]

Figure 2.5.: Decay of $t\bar{t}$ pairs.

Both the W boson and the b quark have lifetimes far below 10^{-10} s and therefore decay already inside the detector.[9] Thus, measuring the mass of the top quarks is only possible by reconstructing them over the energies and momenta of the multiple decay products. For this, the best possible resolution of the detector is required because even small uncertainties in the detection process can lead to a high top-quark-mass uncertainty due to the large amount of involved particles. The capability of the LHC detectors ATLAS and CMS to reconstruct the top-quark mass is estimated[10] to be subject to an uncertainty of 10–20 GeV. Hence, considering equation (2.8), the resolution of the latest particle detectors exceeds the expected top-quark decay width by roughly one order of magnitude.

Because the guideline stated in section 2.3.2, that the resolution should be in the same order of magnitude, cannot be fulfilled, the only way to make a decay width measurement possible is to increase the statistics and to have precise knowledge of the resolution of the used detector.

[9] Even if their velocities were $v \approx c$, they would propagate only a few millimeters before disintegrating.
[10] A Monte-Carlo-algorithm-based simulation by ATLAS determines the resolution of the top-quark mass to be about $\sigma_{\text{det}} = 17$ GeV [39].

3. Experimental Particle Physics at the LHC

With a few exceptions the particles of the SM do not exist in nature at all or at least not as free particles—they have to be produced artificially. For this, the principle of energy-mass equivalence is used: high energies are generated from which (in a simplified representation) new particles arise through statistical processes. To create such high energies, bunches of particles are accelerated to velocities near the speed of light with particle accelerators; in most cases (including the LHC) the accelerators are built in a circular form where the particles are sped up in each round. A second beam is accelerated in the opposite direction to finally bring both bunches to collision.

The particles being created in such collisions at the LHC are detected with the state-of-the-art detectors ATLAS and CMS to precisely reconstruct the final state products of these collisions. The difficulty in the reconstruction is that the majority of the produced particles is unstable, decays already inside the detector, and generates a large amount of lighter particles. Hence, the detector must be able to capture a lot of particles very accurately at the same time to make an exact reconstruction possible. The following sections describe the operation of the LHC and one of the LHC detectors, the ATLAS experiment.

3.1. The Large Hadron Collider (LHC)

The Large Hadron Collider (LHC) is currently the world's most powerful particle accelerator with centre-of-mass energies of $\sqrt{s} = 7\,\text{TeV}$ (2010–2011) and 8 TeV (2012). The LHC is operated by the European Organization for Nuclear Research, shortly CERN (abbreviation of the former French name *Conseil Européen pour la Recherche Nucléaire*) which was established in 1954. CERN currently holds twenty member states. Just like the CERN organization, the LHC is located at the border between France and Switzerland.

The LHC is a circular accelerator with a circumference of 26.7 km. Due to its huge dimensions and to minimize exterior influences (e.g. cosmic radiation), it is located in a

tunnel between 100 and 120 m below ground. The tunnel contains two adjoining beam pipes intersecting at four different points at which the collisions of the two beams take place. Overall, about 1,600 magnets (dipole and quadrupole) are installed to bend the beams to their circular path and to keep them focused. As they are made of superconducting material, their operating temperature is below 2 K so that a large amount of helium is needed to cool the system down. Additionally, in the beam pipes ultrahigh vacuum prevails to prevent the accelerated particles from scattering with gas molecules.

The LHC is mainly focused on proton-proton collisions (although some experiments with lead ions have been made). They are accelerated, focused, and bunched together in multiple pre-accelerator stages; in the LHC, they are accelerated from around 450 GeV per beam to their final energy. In 2010, the operation of the LHC started with around 3.5 TeV per beam, i.e. a total centre-of-mass energy of $\sqrt{s} = 7\,\text{TeV}$.[1] In 2012, the system was upgraded to a centre-of-mass energy of $\sqrt{s} = 8\,\text{TeV}$. Since February 2013, the operation is interrupted for an upgrade which is expected to last until 2015. Then, the maximum design centre-of-mass energy of 14 TeV will finally be achieved.

The amount of collisions per second produced by a collider is usually described in terms of the instantaneous luminosity $\mathcal{L}$ that connects the production rate $\dot{N}$ of a specific type of process with its cross section σ. Since the luminosity is the ratio of both, it is independent from the investigated process.[2] To describe the total amount of collisions, the integrated luminosity $\int \mathcal{L} dt$ is used.

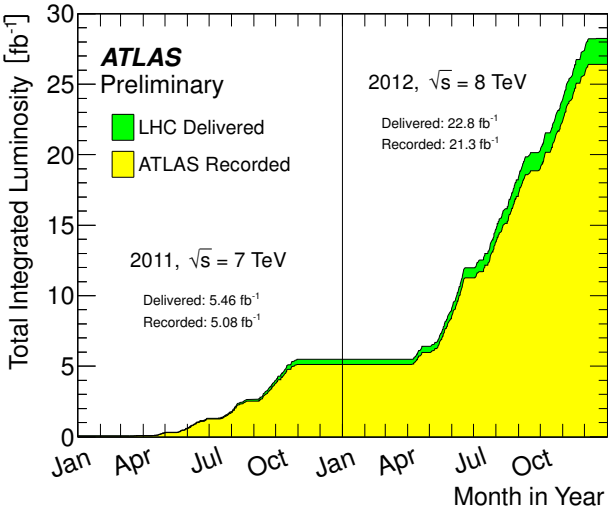

Figure 3.1.: Integrated luminosity of the LHC measured by the ATLAS detector [40].

[1] With this energy, the proton bunches circulate with a frequency of around 11 kHz (11,000 rotations per second) and at a velocity of about $v = c - 3\,{}^{m}/_{s}$.

[2] The luminosity is formally calculated over $\mathcal{L} = \dot{N}/(\sigma A \epsilon)$ where A and ϵ are technical parameters (acceptance A and detecting efficiency ϵ) of the detector used for the measurement.

In figure 3.1, the total integrated luminosity of the LHC runs in 2011–2012 measured by the ATLAS detector is shown. At a centre-of-mass energy of $\sqrt{s} = 7\,\text{TeV}$, the amount of collected data is about $5.08\,\text{fb}^{-1}$ while the 2012 run at $\sqrt{s} = 8\,\text{TeV}$ produced about $21.3\,\text{fb}^{-1}$ of collected data. For comparison, during Run II of the TEVATRON in the years 2001–2011 about $10\,\text{fb}^{-1}$ of integrated luminosity were collected by the CDF collaboration.

All in all, seven experiments are situated at the LHC in which different areas of research are explored. While the two main detectors ATLAS and CMS serve general purposes, the experiments ALICE and LHCb are specialized on investigating heavy ions and b-quark physics, respectively. The three remaining detectors TOTEM, MoEDAL and LHCf cover very specific areas (e.g. LHCf works on issues in the field of astroparticle physics).

3.2. The ATLAS Detector

The ATLAS detector is the largest of the LHC experiments. It is about 44 m long, 25 m in diameter, and weighs approximately 7,000 t. The detector is operated by the ATLAS collaboration in which about 3,000 researchers are involved. The following information is based on the technical design report of the ATLAS detector [41].

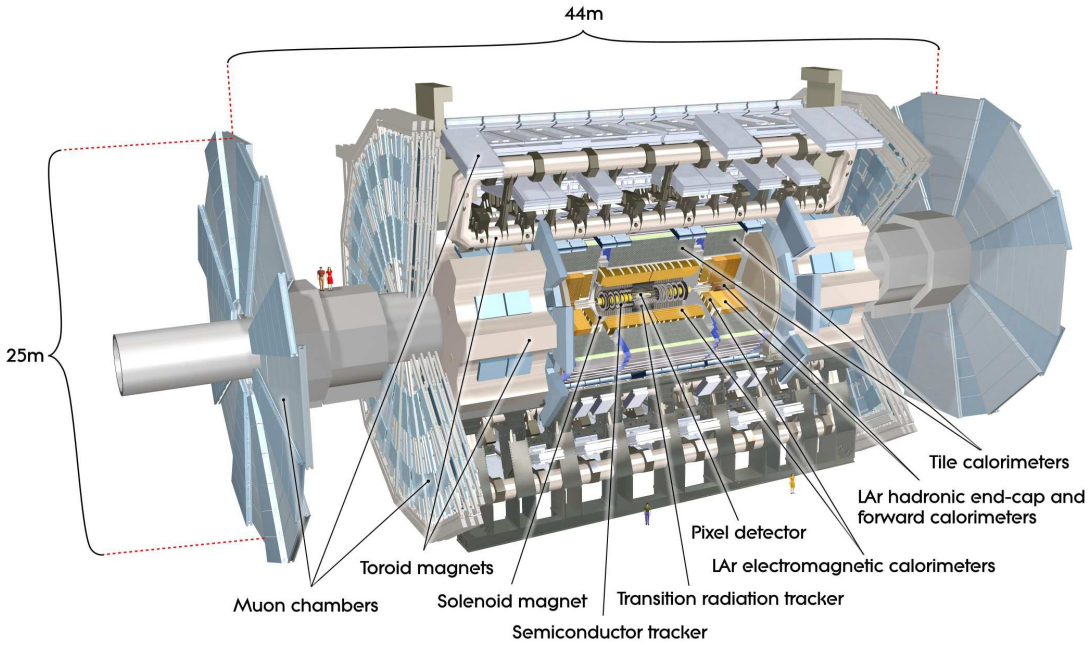

Figure 3.2.: Overview of the structure of the ATLAS detector [42].

Figure 3.2 shows the concentric construction of the detector: The inner detector comprising the pixel detector, the semiconductor tracker, and the transition radiation tracker begins as close to the beam axis as possible, its outer radius is 115 cm. All parts of the

inner detector are designed to measure precisely the direction of the emerging particles. The innermost layer of the inner detector is the pixel detector consisting of a large amount of small pixels, which are triggered when particles pass through. It is designed to provide a high-precision set of measurements; because of its proximity to the interaction point the material has to be radiation-hard. The semiconductor tracker being the middle component of the inner detector is made of strips detecting passing particles. This construction provides a better coverage of larger areas. The transition tracker, which is the outermost layer, is based on the use of straw detectors, i.e. it is composed of wire chambers working with ionization detection.

Around the inner detector, a solenoid magnet system is installed to bend the trajectory of charged particles, so that positively and negatively charged particles can be separated based on the curvature of their tracks. Besides, the degree of curvature gives direct evidence of the momentum of the particles.[3]

Outside the solenoid magnets two sorts of calorimeters are installed: the electromagnetic and the hadronic calorimeter, both serving the purpose of measuring the energy of the particles. They are designed as sampling calorimeters, i.e. they consist of two different layers: a high-density metal to absorb energy and the "measuring" layer, where the deposited energy is determined. While the electromagnetic calorimeter is made of lead and liquid argon (LAr) and is intended to detect particles interacting primarily via the electromagnetic interaction, the hadronic calorimeter consists of plastic scintillator plates embedded in an iron absorber and is able to measure the energy of particles interacting via the strong interaction. The calorimeter region extends up to a radius of about 4.2 m.

The outermost component extending up to a radius of 11 m is the muon spectrometer. A separate system for muons is needed because they pass the calorimeter systems without depositing their energy completely. The system consists of a toroidal magnet system and two muon chamber systems. One of them is designed to measure the tracks of muons with high spatial precision; the purpose of the other is to trigger with an accurate time resolution, when a muon passes. The latter is used to quickly identify events including one or more muons to allow a hardware-based event selection even before storing the measurements on hard disks. The magnet system again bends the trajectories of the muons allowing a precise measurement of their momentum.

[3]Uncharged particles can be distinguished as they do not produce any tracks at all.

4. Establishing a Model for the Decay Width Measurement

In this chapter, the problem of measuring the top-quark decay width is summarized compactly. Besides, techniques and statistical methods are presented that were used for the feasibility studies. As a first approach preliminary studies were done to prepare the sensitivity studies—they can be found in section 4.3. The final section 4.4 then provides an explanation of the steps towards the actual sensitivity studies.

4.1. Defining the Problem

Measuring the top-quark decay width is a very difficult process because it cannot simply be "read" off the width of the mass distribution of the top quark. The distribution of the reconstructed top masses is a convolution of two functions: on the one hand the actual physical distribution, a Breit-Wigner function of the general form [43]

$$f(x;\mu,\Gamma) = \frac{1}{2\pi}\frac{\Gamma}{(x-\mu)^2 + (\Gamma/2)^2} \tag{4.1}$$

defined by its average value μ (here: the top-quark mass m_t) and a parameter Γ describing the width of the distribution (here: the top-quark's natural decay width Γ_t); on the other hand a distribution which describes the resolution of the detector.

> **Definition of a convolution:** If two functions $f, g : \mathbb{R} \to \mathbb{R}$ are absolutely integrable and their Fourier transforms $F(\omega) = \mathcal{F}\{f(t)\}$ and $G(\omega) = \mathcal{F}\{g(t)\}$ exist, then
>
> $$f(t) * g(t) \stackrel{\text{def.}}{=} \int_{-\infty}^{+\infty} f(\tau)g(t-\tau)d\tau \tag{4.2}$$
>
> is the convolution of f and g [44].

In principle, the two functions must be "unfolded" to get a representation of the purely physical Breit-Wigner curve which is only possible with numerical approximations. An-

other way to obtain information on the width of the Breit-Wigner curve is to perform a template fit: on the condition that the two original functions are exactly qualitatively known, the observed convolution is re-calculated to serve as a fit function. Now its different parameters are varied to find the set of parameters that has led most likely to the observed convolution.

However, the estimation of the parameter set via template fitting is very sensitive: Since the most probable set of parameters is merely found by numerical approximation methods, it might happen that the convolution is reproduced correctly, but the values of the parameters don't make any sense in physical terms. In addition, a correct reproduction is less likely, the more parameters are incorporated in the convolution. The use of Bayesian statistics can help to calculate even multi-parameter models: The range of the individual parameter values can be restricted before the actual fitting by introducing prior probability densities.

4.2. Some Basic Concepts of Statistics

This section is intended to give a brief introduction to the statistical terms and concepts used in the subsequent studies and are therefore essential for the understanding and interpretation of the results.

4.2.1. Estimators

A data sample is normally used to gain information about the parent distribution function; for this, calculating procedures are applied to the data sample to get a numerical value for a property of the parent distribution (in the following studies: get a value for the top-quark decay width from a pseudo-data sample). For example, the calculation of a mean value or a standard deviation are such types of procedures. Since every value obtained from a data sample only estimates the true property of the parent distribution, these procedures are called *estimators*. Because not all estimators are as good as others (e.g. adding the lowest and highest value and dividing them by 2 is not a precise estimation of the average mean), there are generally three terms that describe the quality of an estimator [45]:

1. **Consistency:** An estimator $\hat{a}$ is *consistent* if it tends to the true value a as the number of data values n tends to infinity:

$$\lim_{n\to\infty} \hat{a} = a \tag{4.3}$$

2. **Bias:** An estimator is *unbiased* if its expectation value $\langle \hat{a} \rangle$ is equal to the true value:

$$\langle \hat{a} \rangle = a \tag{4.4}$$

3. **Efficiency:** An estimator is *efficient* if its variance is small, i.e. the spread of possible values should be as small as possible.

4.2.2. Fitting

In general, curve fitting of a data sample is the procedure where a distribution function is constructed that fits best to the given data sample. Because curve fitting is nothing more than estimating the parameters of the curve, the used techniques to gain the fitting results are different methods of estimation. In addition to the very popular *method of least squares*, the *principle of maximum likelihood* is very commonly used. For more complex, multidimensional problems, Monte Carlo methods are often applied.

Principle of Maximum Likelihood:

Consider a random variable x distributed according to a distribution function $f(x;\, \varphi)$ with an unknown parameter φ; the objective is to estimate φ. Suppose a measurement of the random variable x has been repeated n times and has led to the values $\{x_1, \ldots, x_n\}$. The *likelihood function* $\mathcal{L}(\{x_i\};\, \varphi)$ is then defined as the combined probability that this particular set of $\{x_i\}$ would be produced from the value φ [43]:

$$\mathcal{L}\left(\{x_i\};\, \varphi\right) \;=\; \prod_i P(x_i|\varphi) \tag{4.5}$$

where $P(x_i|\varphi)$ is the conditional probability of measuring x_i when φ is the value of the unknown parameter that produced the data sample. The principle of maximum likelihood (ML) maximizes this function with respect to the parameter φ:

$$\frac{\partial \mathcal{L}}{\partial \varphi} = 0 \tag{4.6}$$

The value $\hat{\varphi}$, at which eq. (4.6) is fulfilled, is the estimator for the parameter φ, i.e. the principle of maximum likelihood determines the value of φ that makes the probability of the obtained results $\{x_i\}$ as large as possible [45]. The maximum likelihood can be calculated for multi-parameter problems as well: φ becomes $\boldsymbol{\varphi} = (\varphi_1, \ldots, \varphi_m)$ and the

maximization condition expands for $\mathcal{L}(\{x_i\};\, \boldsymbol{\varphi})$ to

$$\frac{\partial \mathcal{L}}{\partial \varphi_j} = 0 \quad \text{where } j = 1, \ldots, m. \tag{4.7}$$

Monte Carlo Methods:

When it comes to multi-parameter problems with very complex structures (e.g. integrating over multiple dimensions), the ML method reaches its limits. In this case, Monte Carlo methods can be used: They are computational algorithms relying on repeated random sampling. With a sufficient number of repetitions, the algorithms yield very precise numerical results. Especially Monte Carlo algorithms based on Markov chains, known as Markov Chain Monte Carlo (MCMC) algorithms, are frequently used tools to approach multidimensional integrals—they determine the samples by running through a Markov chain, i.e. by doing a "random walk". For example, MCMC algorithms are able to approximate probability density functions in multidimensional Bayesian statistics.

4.2.3. Bayesian Statistics

Bayesian statistics uses a different interpretation of the concept of probability known as subjective (or simply: Bayesian) probability. In the Bayesian interpretation, the probability $P(a)$ is often explained as a measure of "degree of belief" that the hypothesis a is true. The entire field of Bayesian statistics is based on Bayes' theorem [45]:

$$P(a|b) \;=\; \frac{P(b|a) \cdot P(a)}{P(b)} \tag{4.8}$$

As described in the last section 4.2.2, $P(a|b)$ is the *conditional* probability that a happens when b is already true. In Bayes' theorem, the probability $P(a)$ is referred to as *prior* probability while $P(a|b)$ is called *posterior* probability.

The theorem can be interpreted as follows: One starts with a certain degree of belief in the hypothesis a, i.e. with the prior probability $P(a)$. If then b becomes true, the degree of belief in a is updated to the posterior probability $P(a|b)$. a could for example be a theory; b could be a data set which yields certain results agreeing or disagreeing with the theory. If the results agree with the theory, the degree of belief in the theory increases. If they disagree with the theory, the confidence in the theory decreases. However, this strongly depends on the probability $P(b) = P(\textit{results})$ that b becomes true at all. If b is very likely for other reasons (e.g. in other theories), b does not provide strong support for the theory a even if the theory predicts b to happen.

4.3. Preliminary Studies: the ML-Fit Approach

In the first preliminary studies the feasibility of the likelihood-fit method was studied by using very simple models. The function describing the detector resolution was set to a simple Gaussian curve (explained in more detail in the following subsection). The observed convolution of this Gaussian and the Breit-Wigner function of the top mass distribution is then a so-called Voigt distribution. Although it has no analytical representation, it can be implemented numerically. In this case, the fitting to the pseudo-data sample using the maximum likelihood estimation is done with only four parameters: the top mass m_t as the expectation value of the distribution, the decay width Γ_t, the detector resolution σ_{det}, and a scaling factor that adjusts the height of the normalized Voigt function to the size of the data sample. Since the data sample is binned in a histogram with a certain number of bins, the model parameter "bin width" d also has an influence on the result.

For each of the initial studies, $n_{\text{spectra}} = 10{,}000$ pseudo-data samples were generated. These spectra were analyzed with a ML fit to obtain a fitted value for Γ_t. Afterwards, the fit results for Γ_t of the whole set of spectra were binned to a histogram and their mean, their standard deviation, and their uncertainty were calculated.

4.3.1. Setting the Input Values of the Parameters

For the preliminary studies, the following initial values for the parameters were chosen:

$$m_t = 174.0\,\text{GeV} \tag{4.9a}$$

$$\Gamma_t = 2.0\,\text{GeV} \tag{4.9b}$$

$$\sigma_{\text{det}} = 30.0\,\text{GeV} \tag{4.9c}$$

$$d = 0.6\,\text{GeV} \tag{4.9d}$$

The top-quark properties m_t and Γ_t were roughly set to values near their estimated physical values (see eq. (2.6) and (2.8) in the theory chapter). The bin width d results from the fact that the used histogram had a range of 0–300 GeV with 500 bins.

For the detector resolution, a recent ATLAS publication was consulted in which the top-quark mass had been measured with the template method [46]. The measured top-quark-mass distributions (of two different channels) are shown in the upper plots in figure 4.1. For comparison, a Monte Carlo simulation of the expected sample distribution is plotted as well. In the lower plots, the data points and the used fitting functions are shown. ATLAS used a Gaussian distribution to approximate the top-quark-mass peak and a Landau

distribution to approximate the background events. For simplicity, these background events were not considered in the initial studies.

The width of the Gaussian distribution is dominated by the uncertainties in the top-quark-mass measurement. One main issue in measuring m_t is the large amount of particles involved in the reconstruction, especially the b quarks and the quarks of hadronically decaying W bosons as they produce jets of more particles. Since the measurement of their energy and momentum is subject to uncertainties (mainly due to restrictions of the calorimeters), they produce an uncertainty in the reconstruction of m_t called jet energy scale (JES). The JES is predominantly responsible for the parameter "σ_{det}". To create a large discrepancy to $\Gamma_t = 2\,\text{GeV}$, in the initial studies σ_{det} was set to 30 GeV.

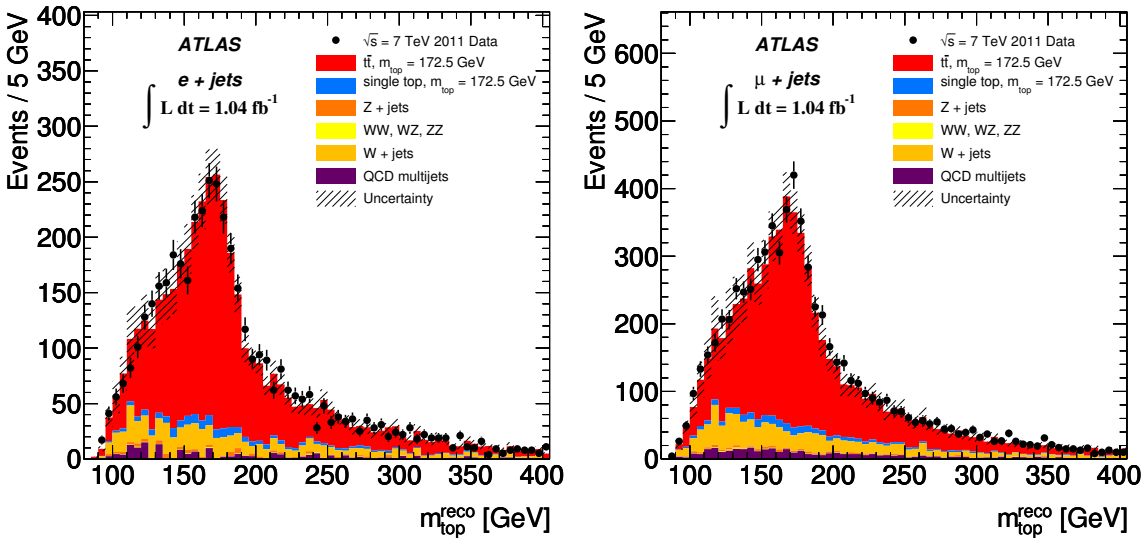

(a) electron+jets channel (b) muon+jets channel

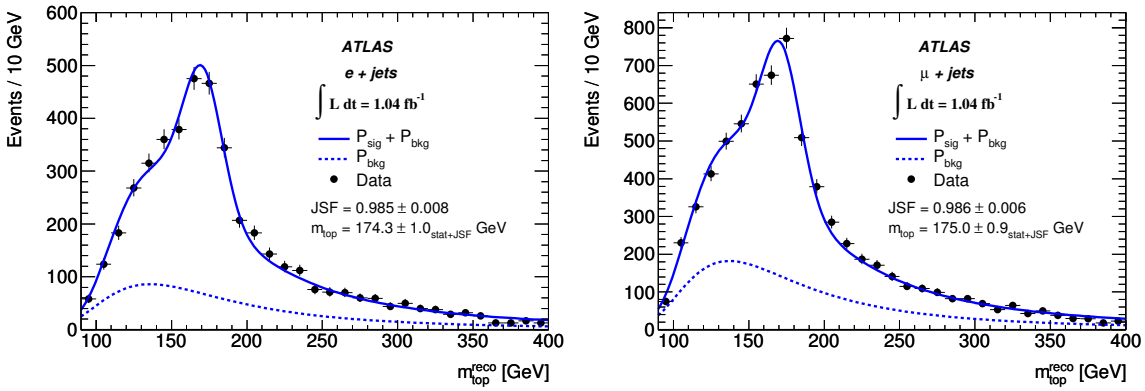

(c) electron+jets channel (d) muon+jets channel

Figure 4.1.: Distribution of the reconstructed top-quark mass in a $\sqrt{s} = 7\,\text{TeV}$ analysis in a recent ATLAS publication [46]. The upper plots show the reconstructed data samples and the Monte-Carlo-based SM predictions. In the lower plots the data is plotted against the used fit function.

4.3.2. Studies of the Convolutions of Gaussian and Breit-Wigner Functions

In a first study, the convolution of a Gaussian and a Breit-Wigner function was simulated. To obtain a good reproducibility of Γ_t, the model was used with the strong constraint that the top-quark mass and the detector resolution are fixed and therefore cannot be varied during the fitting. The values of the parameters, with which the pseudo-data spectra were created, were set as described in eq. (4.9). The number of events n_{events} in each of the spectra was set to 30,000.

In figure 4.2 the fitted values of Γ_t and the associated relative uncertainties of Γ_t are plotted. The plots show that the initial value of 2.0 GeV is reproduced very well: the calculated average of 10,000 spectra is 1.988 GeV and deviates thereby only by -0.6% from the input value. At the same time, the uncertainty on this mean average is $0.19\,\text{GeV}/\sqrt{n_{\text{events}}} \approx 0.02\,\text{GeV}$. The relative uncertainty of the fitted values of Γ_t is on average 9.7% with a small dispersion of about $\pm 0.7\%$.

4.3.3. Studies of the Convolutions of Two Gaussian Distributions

As an alternative to the theoretically expected Breit-Wigner curve, a Gaussian distribution was used in a second preliminary study to approximate the top-quark mass distribution. This step can be justified because the much broader curve describing the detector resolution quantitatively determines the shape of the convolution anyway—a Gaussian curve is almost indistinguishable from a Breit-Wigner curve in the resulting convolution because their impact on the shape is so small.

The approximation with a Gaussian curve has the great advantage that a convolution of two Gaussian distributions can be mathematically described very well: Gaussian functions are *invariant* under convolution; thus, a convolution of two Gaussian distributions yields again a Gaussian distribution. The convolution h of two functions f, g with mean x and standard deviations σ_f and σ_g is simply denoted as follows:

$$h(x) = f(x) * g(x) \quad \text{where} \begin{cases} f(x) = \text{Gauss}(x;\ x_0,\ \sigma_f), \\ g(x) = \text{Gauss}(x;\ x_0,\ \sigma_g) \end{cases} \tag{4.10}$$

$$\Rightarrow \quad h(x) = \text{Gauss}\left(x;\ x_0,\ \sigma_h = \sqrt{\sigma_f^2 + \sigma_g^2}\right) \tag{4.11}$$

Applied to the problem, this means that the observed standard deviation of the convo-

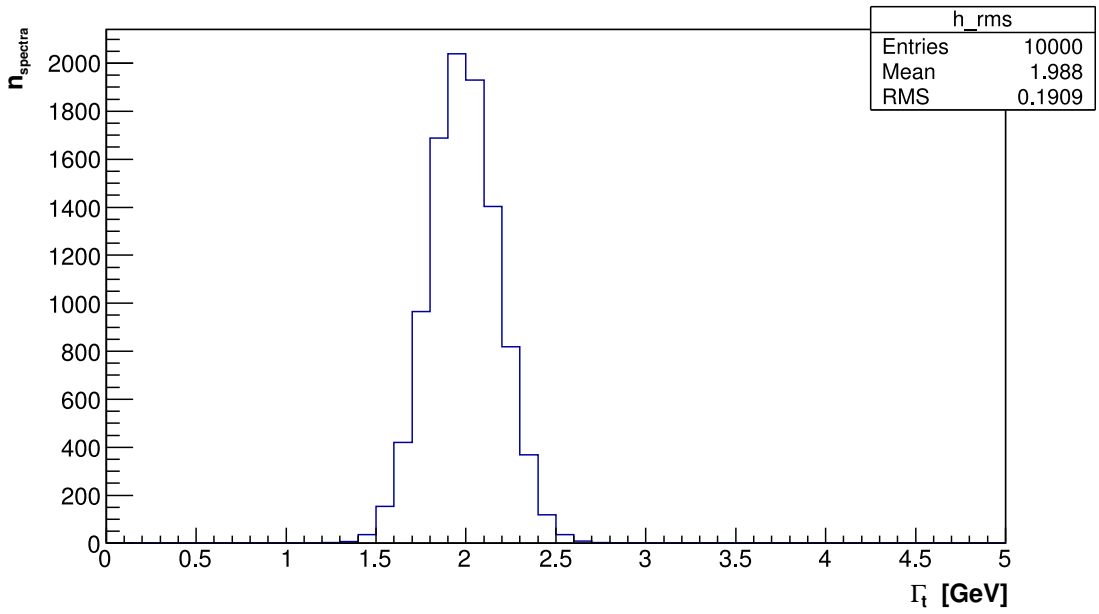

(a) The fitted values for the decay width Γ_t

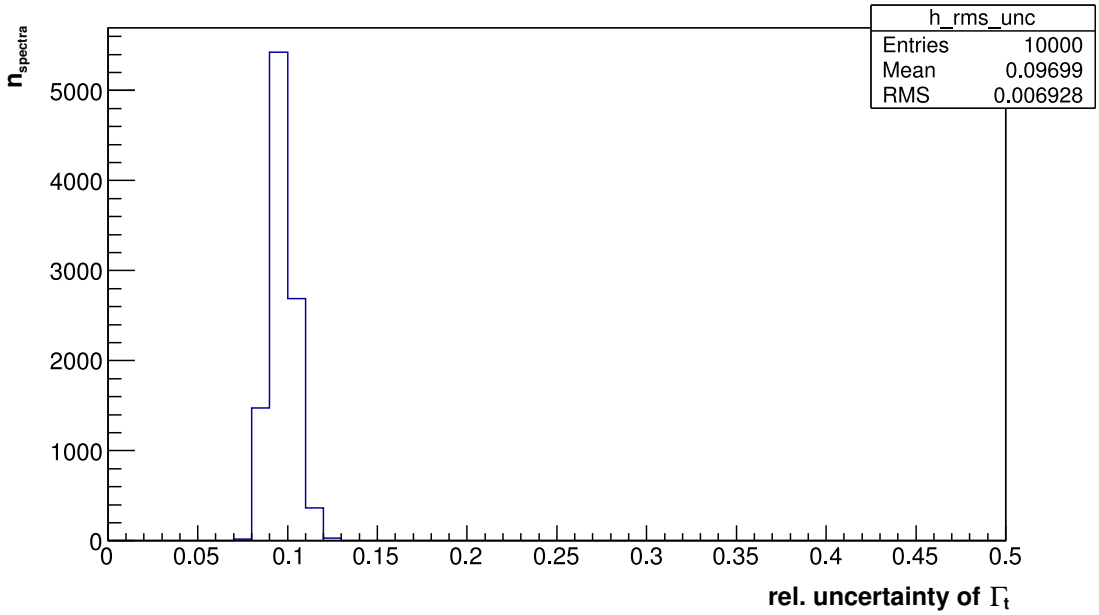

(b) The corresponding relative uncertainties

Figure 4.2.: Results of the convolution of a Gaussian and a Breit-Wigner function.

lution is $\sigma_{\text{tot}} = \sqrt{\sigma_{\text{det}}^2 + \sigma_t^2}$, the top-quark standard deviation[1] is $\sigma_t \approx 0.85\,\text{GeV}$. In the following preliminary consideration, an estimator for Γ_t is calculated using this formula. The estimator makes it possible to estimate the sample size n_{events} required for achieving a certain relative uncertainty of Γ_t.

Estimating the Decay Width

If the size of the data sample (i.e. the number of events n) and the detector resolution σ_{det} is known, the decay width Γ_t (or the corresponding standard deviation σ_t) can be reconstructed by using the fit results. If the data is observed to be Gaussian distributed with a standard deviation σ_{data}, σ_t can then be estimated by

$$\hat{\sigma}_t = \sqrt{\sigma_{\text{data}}^2 - \sigma_{\text{det}}^2} \tag{4.12}$$

according to eq. (4.11). Since σ_{det} is known, only σ_{data} is subject to uncertainty. Considering the propagation of uncertainties[2] , the uncertainty on $\hat{\sigma}_t$ therefore yields:

$$\sigma[\hat{\sigma}_t] = \sqrt{\sigma^2[\sigma_{\text{data}}] \cdot \left(\frac{\partial \hat{\sigma}_t}{\partial \sigma_{\text{data}}}\right)^2} = \sigma[\sigma_{\text{data}}] \cdot \frac{\sigma_{\text{data}}}{\hat{\sigma}_t} \tag{4.13}$$

The uncertainty on the uncertainty of the estimator for Gaussian distributed variables tends to $\sigma[\hat{\sigma}] = {}^{\hat{\sigma}}/_{\sqrt{2n}}$ for large data samples [45]. Substituting $\sigma[\sigma_{\text{data}}]$ in eq. (4.13), this leads to:

$$\sigma[\hat{\sigma}_t] = \frac{1}{\sqrt{2n}} \cdot \frac{\sigma_{\text{data}}^2}{\hat{\sigma}_t} \tag{4.14}$$

Using this equation, the minimum size of a data sample needed for achieving a certain relative accuracy of σ_t can be estimated. Should this be for example 10% and the mass resolution is $\sigma_{\text{det}} = 30.0\,\text{GeV}$, this would result in $\sigma_{\text{data}} \approx 30.07\,\text{GeV}$ and a data sample

[1] For Gaussian distributions, the standard deviation is about 2.35 times the *FWHM* (exactly: $2\sqrt{2\ln 2}$). With a decay width of $\Gamma_t = 2.0\,\text{GeV}$ this leads to $\sigma_t = {}^1/_{2.35} \cdot \Gamma_t \approx 0.85\,\text{GeV}$.

[2] If a function $f = f(x_1, x_2, \ldots, x_n) = f(\{x_i\})$ depends on the variables $\{x_i\}$, which are subject to uncertainties σ_{x_i} (where $1 \leq i \leq n$), the uncertainty of the function f is calculated as follows [44]:

$$\sigma_f = \sqrt{\sum_{i=1}^{n} \left(\sigma_{x_i} \cdot \frac{\partial f}{\partial x_i}\right)^2} = \sqrt{\left(\sigma_{x_1} \cdot \frac{\partial f}{\partial x_1}\right)^2 + \left(\sigma_{x_2} \cdot \frac{\partial f}{\partial x_2}\right)^2 + \cdots + \left(\sigma_{x_n} \cdot \frac{\partial f}{\partial x_n}\right)^2}$$

with the following number of events would be needed:

$$n \;>\; \frac{1}{2} \cdot \left(\frac{\sigma_{\text{data}}}{\hat{\sigma}_t}\right)^4 \cdot \left(\frac{\hat{\sigma}_t}{\sigma[\hat{\sigma}_t]}\right)^{-2} \approx 2.5 \cdot 10^6 \tag{4.15}$$

Results of the Fit

Using the estimated size of the data sample in eq. (4.15) the convolution of two Gaussian distributions was simulated with a set of pseudo-data spectra as well. Again, m_t and σ_{det} were fixed during the fit while the other initial parameters were set to the same values as stated in eq. (4.9). For the calculation, the top-quark decay width Γ_t was converted to σ_t—the results were then reduced by the corresponding factor again. Figure 4.3 shows the determined values for Γ_t from 10,000 spectra and the corresponding relative uncertainties.

The histograms show that the decay width can only be reproduced with a much larger variance compared to the previous model. Although the average mean of about 2.02 GeV deviates only by 1.1% from the initial value, the relative uncertainty is almost 21% and has a dispersion of ±10.4%. One of the reasons for the dispersion is that the distribution is strongly skewed to the right. This happens mainly due to very small values of Γ_t for which the relative uncertainty increases rapidly even if its absolute value is not increased compared to larger values of Γ_t.

Noteworthy is also the fact that the calculation of Γ_t or σ_t with the use of eq. (4.12) does not work when $\sigma_{\text{det}} > \sigma_{\text{data}}$ (the root in the equation yields a complex value). For the evaluation, these cases were sorted out in advance; therefore, the histograms contain only about 73% of the 10,000 spectra.

Approach with Variances

To circumvent the problem of the root yielding possibly a complex value, a third model with a slightly modified template fit was created so that it contains the variances instead of the standard deviations of the individual Gaussian distributions. For them,

$$V_{\text{tot}} = V_t + V_{\text{det}} \tag{4.16}$$

applies which leads to negative values of V_t in the case that $V_{\text{det}} > V_{\text{tot}}$. Since these calculations are physically meaningless, a further discussion of them is omitted in this section. The corresponding histograms can be found in figure A.1 in the appendix.

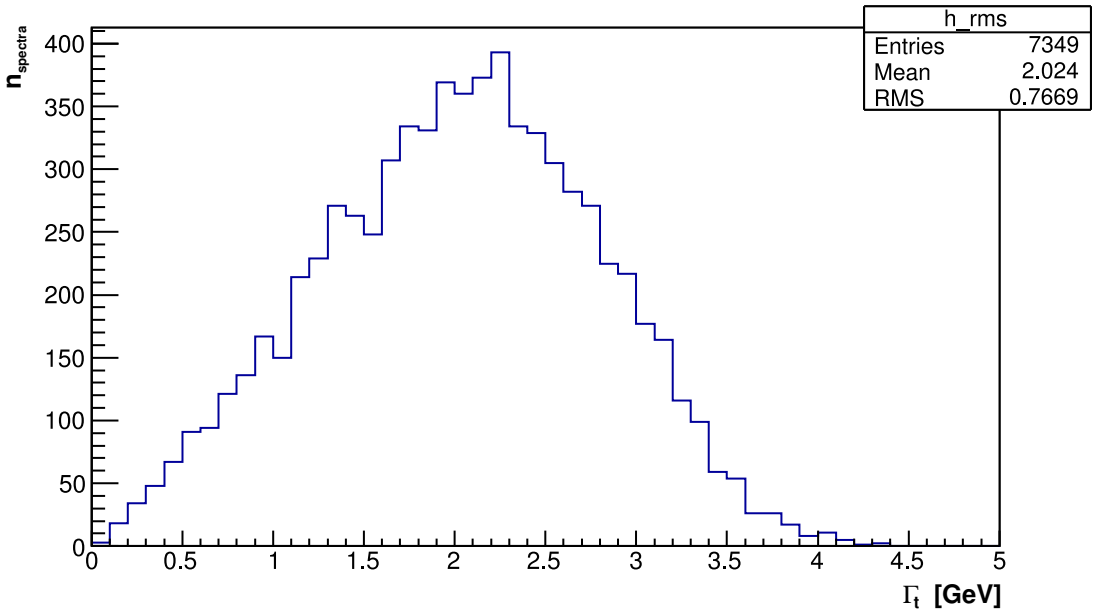

(a) The fitted values for the decay width Γ_t

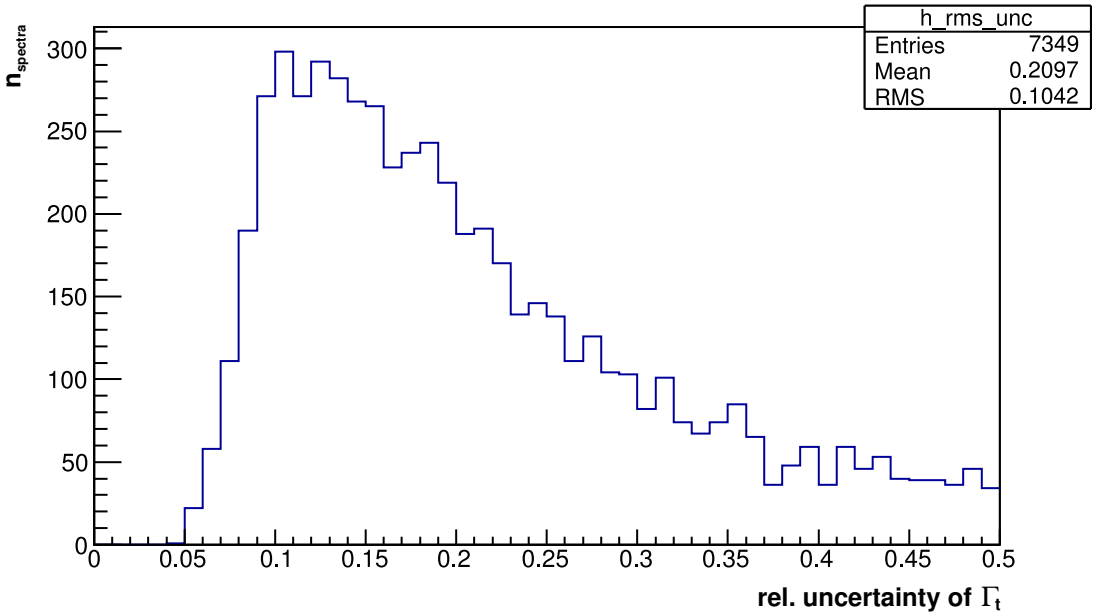

(b) The corresponding relative uncertainties

Figure 4.3.: Results of the convolution of two Gaussian functions.

4.4. The Template-Fit Approach

After the reconstruction of Γ_t had been successful in the preliminary studies (with the highly simplified models), the model for the actual sensitivity studies was extended in some places: In reality it is not possible to cut out only $t\bar{t}$ events and to examine them completely separated because these signal events are always paired with background events having the same signature as $t\bar{t}$ production although originating from different processes. To make the model more realistic, a second function was added to the pseudo-data generation describing that background data. As described in section 4.3.1, a Landau distribution was chosen (see figure 4.1). The shape of the Landau function was linearly linked to the value of m_t but was fixed in its form. Adding background data like this introduces only one additional parameter to the model which adjusts the height of the Landau function to the number n_{bg} of background events as a scaling factor.

Furthermore, the following sensitivity studies were calculated with *conditional* probabilities, i.e. with the use of Bayes' theorem (see eq. (4.8)). For the fitting, not the maximum likelihood estimation, but an MCMC algorithm was used (more accurately: the Metropolis method). The parameters m_t and σ_{det}, previously fixed in the preliminary studies, could now be included in the fit without allowing their full range of values (e.g. the situation could be simulated that the detector resolution is known with an uncertainty of $\pm 2.0\,\text{GeV}$).

Finding the Default Settings

In order to establish a common starting point for the different sensitivity studies, in which the various parameters were varied, a default parameter set was determined. Two conditions were required of this default set: First of all, the fit had to converge with a very high probability, i.e. the algorithm finds the "correct" values for the parameters and does not stop the fitting process after a certain calculation limit without convergence. Second, the model had to be sensitive with respect to Γ_t and had to reproduce it correctly. The latter criteria was demanded because, while performing the calculation of the sensitivity studies, the situation occurred that Γ_t was reproduced with high precision, but on an incorrect value so that the initial value was practically eliminated as a result. The problem is discussed in more detail in the results section 5.3 of the corresponding study.

The size of each spectrum was set to the following event numbers:

$$n_{\text{signal}} = \quad 2.5 \cdot 10^6 \tag{4.17a}$$

$$n_{\text{bg}} = \quad 0.5 \cdot n_{\text{signal}} \tag{4.17b}$$

The number of signal events was set to the value which was calculated in the preliminary studies in section 4.3.3 to achieve an inaccuracy of the decay width of 10%. The used signal-to-background ratio (short: S/BG ratio) of 2:1 corresponds to a very good $t\bar{t}$ event selection in real data.

The physical parameters were set to the following default values:

$$m_t = 172.5\,\text{GeV} \quad \text{(fixed)} \tag{4.18a}$$

$$\Gamma_t = 2.0\,\text{GeV} \tag{4.18b}$$

$$\sigma_{\text{det}} = 20.0\,\text{GeV} \quad \text{(fixed)} \tag{4.18c}$$

$$d = 0.5\,\text{GeV} \tag{4.18d}$$

The chosen top mass corresponds to the default value implemented in the Monte-Carlo event generators for particle physics. As in the initial studies, the top-quark decay width was set to 2.0 GeV which is around the value of the theoretical prediction (eq. (2.8)) and close to the values of the previous measurements (see eq. (2.9) and (2.10)). The detector resolution was fixed to 20 GeV which is in the expected range of the reconstruction uncertainty of the top mass at the ATLAS detector (see section 2.3.3 for more details).

Sensitivity Studies

Based on the default values specified in eq. (4.18) single parameters were varied during the ensuing sensitivity studies in order to find out to what extent the altered parameters affect the reconstructed value of Γ_t. In the subsequent order, the following parameter variations were done:

1. **Variation of the histogram binning:** To test out the model itself, the bin width d of the histogram was varied. Since the default value was set to $d = 0.5\,\text{GeV}$, the variable was varied in a range of 0.1–10.0 GeV.

2. **Variation of the initial decay width:** The initial decay width, with which the pseudo-data spectra were created, was varied between 0 GeV (i.e. non-existent) and 10 GeV. This sensitivity study was important inasmuch as it could help to detect possible biases of the model in the reconstruction of Γ_t.

3. **Variation of the statistics:** In this study, the number of total events was varied from 10^4 to 10^7 (exactly: 10,000–30,000,000). This S/BG ratio was kept constant at all values. With analyzing these spectra, predictions for low- and high-statistical settings could be made (e.g. making predictions for centre-of-mass energies of 7–8 TeV and 14 TeV at the LHC).

4. **Variation of the S/BG ratio:** A high S/BG ratio was expected to lead to a more precise measurement of all parameters including Γ_t. With a default value of 2:1, the ratio was varied between 1:10 and 10:1.

5. **Variation of the detector resolution:** The parameter σ_{det} was expected to have a strong influence on the reconstructed decay width. σ_{det} was varied in the range 0–50 GeV with a default value of 20 GeV.

6. **Variation of the prior width of the detector resolution:** This study simulated the "degree of knowledge" about σ_{det} and served as a prototype for systematic uncertainties in the model. A well-known detector resolution, i.e. a small prior width, was expected to lead to a precise measurement of the decay width.

7. **Variation of the top mass:** Even though the top mass is already very accurately measured (see eq. (2.6)), this sensitivity study was of special interest because it also simulated systematic uncertainties (like the JES) that have strong impact on the obtained results. In this study, the initial top mass was varied between 170 and 175 GeV while the top mass implemented in the fit was fixed at the default value of 172.5 GeV.

5. Results of the Sensitivity Studies

In this section the results of the sensitivity studies listed in the previous section are presented. In the first part, the results of a single data spectrum are explained in detail based on the default parameter set. In particular, the posterior probabilities of the individual parameters are shown.

For each parameter setting, a set of 200 data spectra was created and fitted. Since in every sensitivity study one of the parameters was adjusted to 10–15 different values (for all the other parameters, the default values were used), about 2000–3000 spectra per study were created. In section 5.2 of this chapter, the evaluation of one of these sets of data spectra is discussed. Additionally, the section explains the steps towards the evaluation plots of the sensitivity studies. In the following sections, the evaluation plots of the studies are shown and their results are discussed.

5.1. Example of a Single Data Spectrum

For the default setting (see eq. (4.18)), the parameters of the top-quark mass m_t and the detector resolution σ_{det} were fixed; consequently, the fit was performed with only three parameters (Γ_t and the two scaling factors for signal and background). For one example, the data points and the fit function are shown in the left-hand plot in figure 5.1. The posterior distribution of Γ_t can be found at the right-hand side, the distributions of the scaling factors are in figures A.2 and A.3 in the appendix. These posterior distributions represent the *marginal* probability densities, i.e. projected from the 3-dimensional parameter space onto one dimension; also included are the intervals containing 68.3%, 95.5% and 99.7% of the values. In addition, the global mode, i.e. the global maximum of the posterior probabilities (taking all parameters into account) is indicated as well.

While the two scaling factors look very Gaussian, the shape of the Γ_t distribution is highly non-Gaussian. One of the reasons for this is that $\Gamma_t = 0\,\text{GeV}$ was set as the lower limit for the parameter value in the model and therefore the probability densities are cut-off. Besides, it can be seen that neither the global nor the local mode agree with the true value of 2.0 GeV which is slightly outside the 68% interval. However, all these points

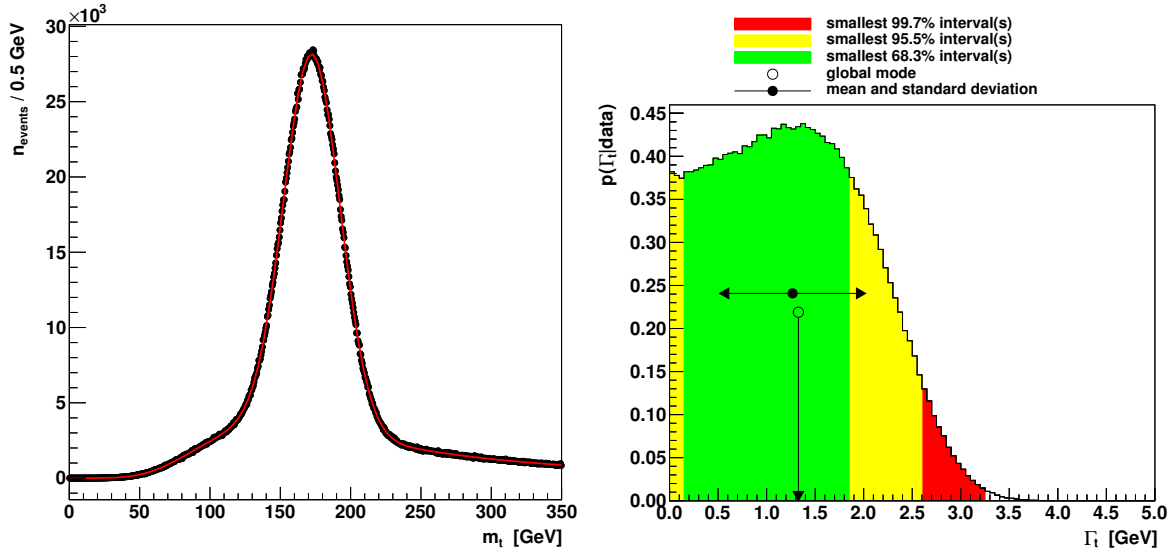

(a) Data sample and fit function (b) Marginalized distribution of Γ_t

Figure 5.1.: Evaluation of a single data spectrum.

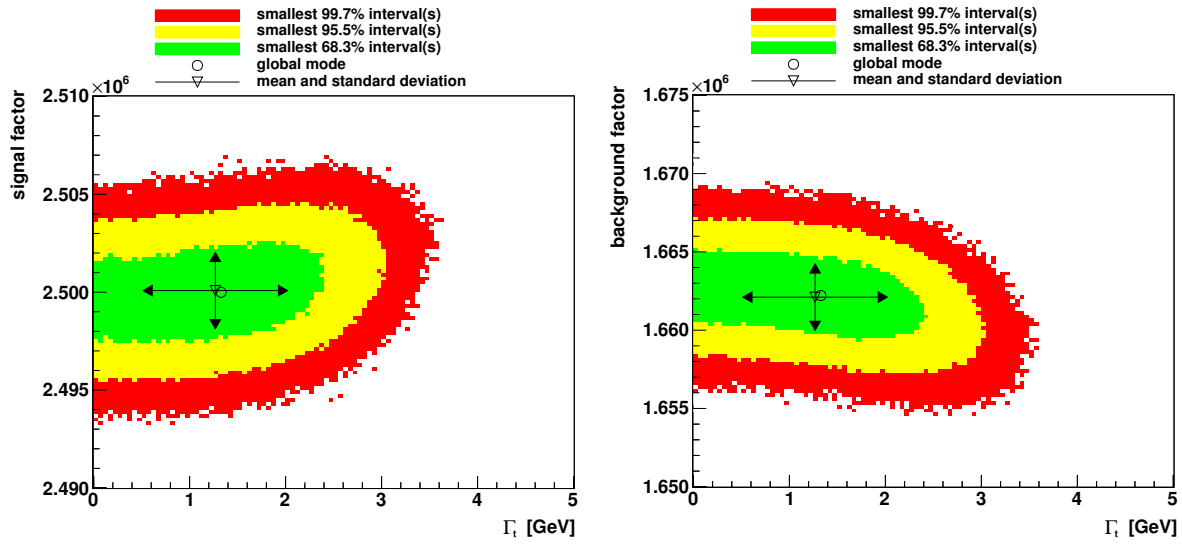

(a) with the signal scaling factor (b) with the background scaling factor

Figure 5.2.: Two-dimensional plots of the correlation between Γ_t and the scaling factors.

are acceptable as they are part of statistical fluctuations as shown in the later studies.

In addition, two-dimensional plots were evaluated in which two parameters were plotted against each other in order to examine their correlation. The plots showing the scaling factors plotted against Γ_t can be found in figure 5.2. The two scaling factors are naturally strongly anti-correlated, for the sake of completeness the corresponding plot A.4 can be found in the appendix.

Figure 5.2 shows that Γ_t is slightly correlated with the scaling factor of the signal events. This can be explained by the fact that the used fit function is normalized, i.e. the height of the function decreases with an increase in the decay width. The other way around, the scaling factor decreases with smaller decay widths because the distribution automatically increases due to its normalized amplitude. The opposite reasons lead to the observed slight anti-correlation of Γ_t with the background scaling factor.

5.2. Example of the Evaluation of a Set of Spectra

This section is supposed to describe the evaluation of the sets of spectra in the sensitivity studies. As described, for each parameter constellation 200 spectra were generated. From each spectrum (e.g. the decay width spectrum in figure 5.1) the mean value and the mode were extracted. Additionally, the quantiles containing a certain amount of data points (e.g. the 90% upper limit or the 68% interval) were saved. The extracted values of the 200 spectra were now averaged. As an example, the figure 5.3 shows a histogram containing the mean values of 200 spectra at the default parameter set.

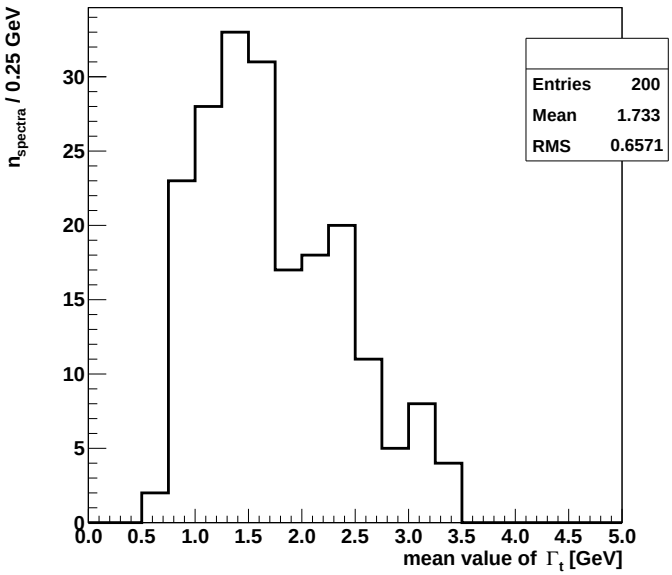

Figure 5.3.: Histogram of the mean values of Γ_t of 200 data spectra.

As these calculations are done for several sets of parameters in which one of them is varied, an evaluation plot of the corresponding sensitivity study is obtained. In this evaluation plot, the averaged values for each step are indicated (and connected with lines to interpolate the areas between the steps). By considering the two independent estimators "mean" and "mode", a possible bias of one of them can be detected immediately. Additionally, the quantiles are used to estimate the uncertainties and the fluctuation of the values.

5.3. Variation of the Histogram Binning

To test the properties of the used model itself, the bin width d of the pseudo-data histogram, i.e. the number of bins, was varied. Since the initial value was set to $d = 0.5\,\text{GeV}$, the range of alteration was chosen to be 0.1–10.0 GeV. The results are shown in figure 5.4. Contrary to the other studies, the number of calculations per step was increased from 200 to 500 to minimize the strong statistical fluctuations observed in a first evaluation.

The plot shows two extremes: for values above 1 GeV the estimated uncertainty of Γ_t decreases, but the expected estimated value becomes smaller. At values above $d = 3\,\text{GeV}$ the initial value of $\Gamma_t = 2.0\,\text{GeV}$ is even excluded from the calculated 95% upper limit. This can be explained by the fact that the bin width heavily affects the capability of the model to reproduce Γ_t when its value is at or above the same value of Γ_t (specifically: the bin width becomes so large that Γ_t is "swallowed" by the histogram bins). On the other hand, the plot shows that the reconstructed decay width does not improve significantly with bin widths smaller than about 0.7 GeV.

5.4. Variation of the Initial Decay Width

In this study the initial value of the decay width, with which the pseudo-data samples were created, was varied. Including the default setting of 2.0 GeV the range was chosen to be 0–10 GeV. In the "interesting" area between 1 and 2 GeV, where the real decay width is expected (see eq. (2.8)), the step size was reduced to obtain more precise results. The evaluation plot is found in figure 5.5.

First of all, the estimated decay width corresponds to the input values very well in the area above 4 GeV. The 68% band becomes narrower with increased values of Γ_t as well. This happens due to the fact that Γ_t and σ_{det} become more distinguishable for higher values of Γ_t since they get in the same order of magnitude.

On the other hand the band widens for smaller values to a maximum of about 1.5 GeV. The interesting thing is that both estimators stagnate at values of about 1.0 GeV which leads to the observation that for input values of 0 GeV and 1 GeV the estimates are nearly indistinguishable. This can be explained with the strict limitation of Γ_t to values above 0 GeV: The marginalized distribution of Γ_t "accumulates" slightly above 0 GeV and can only fluctuate to higher values. This causes the distribution to maintain a certain width and therefore a "slowdown" of the decrease of the mean value. The stagnation of the mode is mainly produced by its large fluctuations in the different data samples caused by the large discrepancy between Γ_t and σ_{det}.

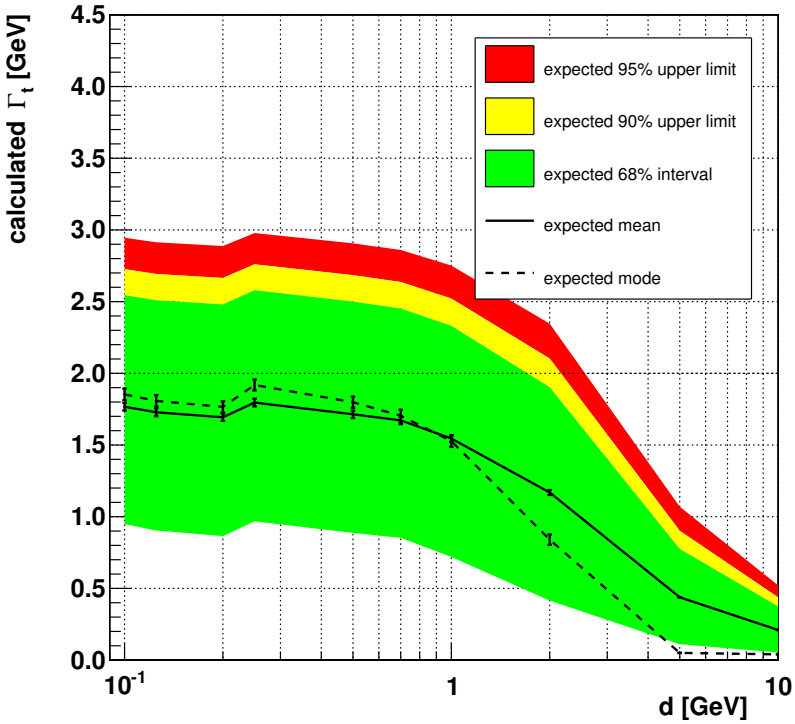

Figure 5.4.: Results of the study in which the bin width d was varied.

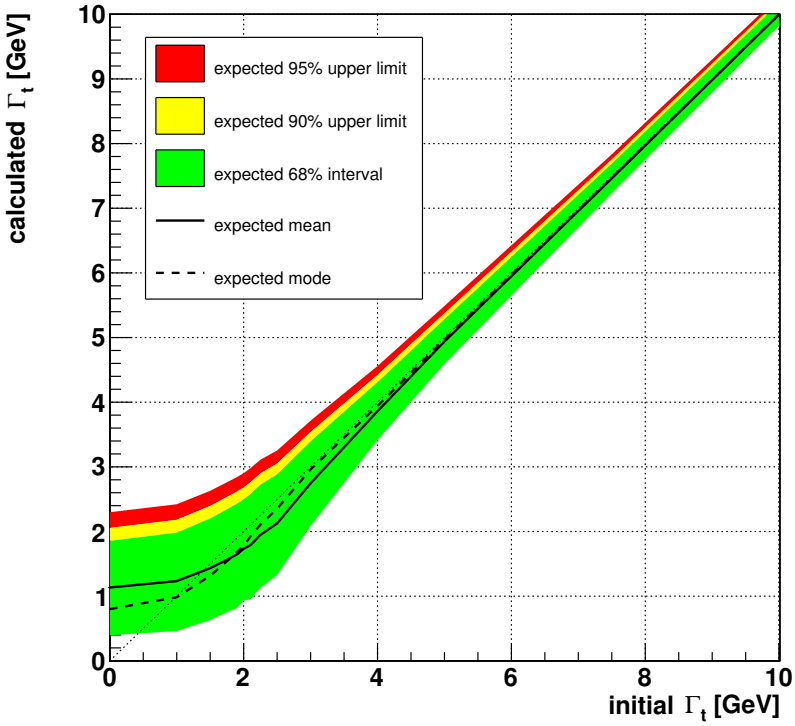

Figure 5.5.: Evaluation plot of the sensitivity study in which the input value of the decay width was varied. In order to maintain the clarity, the data points as well as their error bars are not displayed.

5.5. Variation of the Statistics

In this study, the number of total events was varied from 10^4 to $3 \cdot 10^7$ including the default value of $3.75 \cdot 10^6$. To keep a constant S/BG ratio, both the signal and background levels were altered accordingly. The results are shown in figure 5.6.

As expected, the plot shows that the band of the 68% interval narrows drastically with an increasing number of events. In the complete range, the initial value of $\Gamma_t = 2.0\,\text{GeV}$ is included in the 68% interval. Above approximately 10^6 total events, both estimators reproduce the decay width almost correctly with a very small deviation. However, both estimators are strongly biased for a smaller amount of total events. At around 50,000 events, the expected mode and mean are both more than 50% above the initial value.

This increase for small numbers of events can again be explained with the strict limitation $\Gamma_t > 0\,\text{GeV}$: With low statistics, the marginalized distributions of the parameters widen a lot. Since the distribution of Γ_t is restricted to values above 0 GeV, this causes a higher mean value than for small fluctuations. Additionally, a very wide distribution does not have a single narrow peak, but a broad range of values where the distribution peaks (an example for a very broad distribution of Γ_t can be found in figure 5.7). Since the algorithm used to determine the mode just picks the histogram bin with the highest value, the value of the mode is subject to heavy fluctuations as well. In connection with the limitation $\Gamma_t > 0\,\text{GeV}$ this leads to an increase in the average mode as well.

The shape of the evaluation plot confirms the expectation that the model becomes insensitive to the decay width for low statistics. At a certain point (around 10^6), the necessary size of the data sample is reached so that the reproduction of the decay width works correctly and only the uncertainties keep decreasing.

5.6. Variation of the S/BG Ratio

This study was done to answer the question how good the separation of signal and background must be to gain precise results for Γ_t. For this, the S/BG ratio was varied in the range between 1:10 and 10:1; the default value was originally a ratio of 2:1. Because varying both the signal and the background event numbers would cause multiple effects, this alteration of the ratio was done by varying the background event numbers while the signal events were kept at a constant value. The evaluation plot is found in figure 5.8.

The plot shows no unexpected features. Of course, the width of the 68% interval increases for lower S/BG ratios from its best value of about 1.5 GeV to approximately 2.5 GeV, but both estimators reproduce the decay width correctly with small, but constant

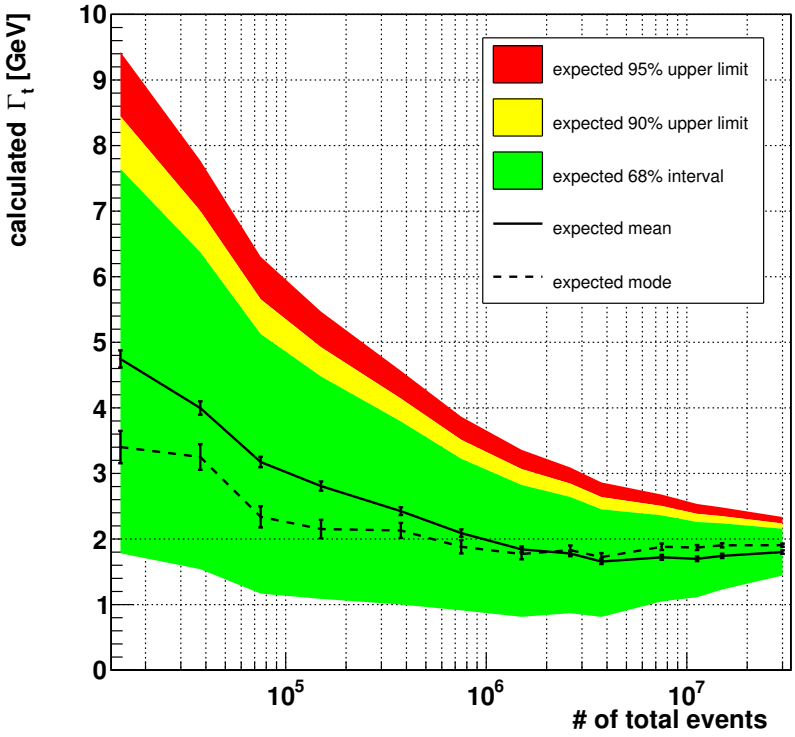

Figure 5.6.: Evaluation plot of the sensitivity study in which the statistics were varied.

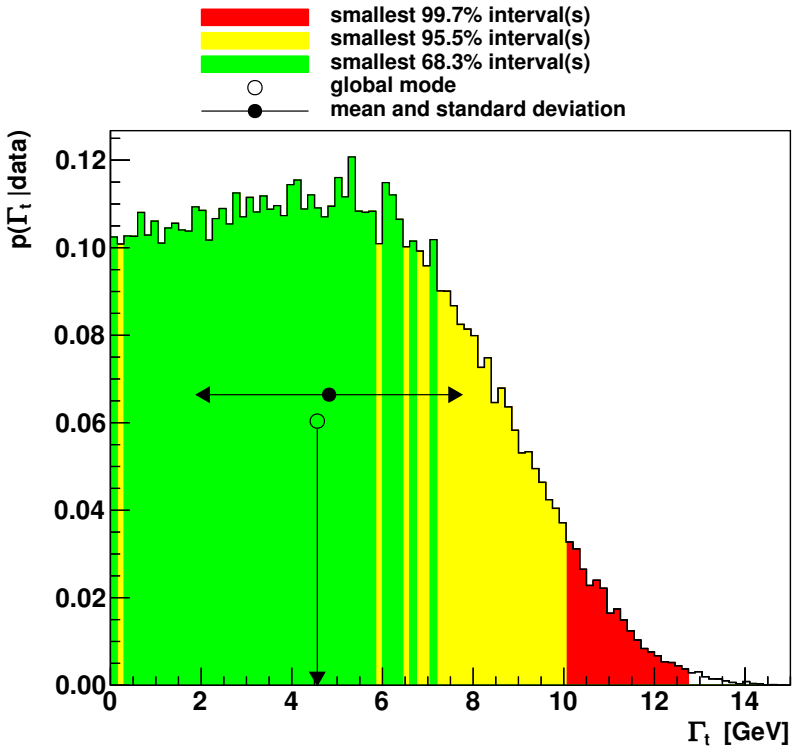

Figure 5.7.: Example for a broad marginalized distribution where the mean value and the mode tend to higher values. The plot was produced with a data sample of 10,000 events.

fluctuations of about 5%. They have increased values at the minimum ratio of 1:10, but this effect is not significant considering the normal statistical fluctuations.

Noteworthy is the fact that both estimators tend to reproduce the decay width slightly too small compared to the initial value. This effect was also observed in the first study (where the bin width was varied) and could probably be a model-based bias.

5.7. Variation of the Detector Resolution

This study investigated the question to what extent a change in the detector resolution could have an effect on the estimated decay width. Because both of these parameters are included in the convolution function equally, the expectation is that the precision of the measurement of Γ_t changes a lot with a varied detector resolution. The range of variation, that can be seen in figure 5.9, comprises 0–50 GeV which includes the default value of 20 GeV.

The graph shows exactly the expected shape. While for $\sigma_{\text{det}} \to 0\,\text{GeV}$ the determination of Γ_t becomes extremely precise, for large values the model becomes significantly less sensitive to the decay width. Both estimators show little fluctuations; above 30 GeV the expected mean value tends to values larger than 2.0 GeV. Noteworthy is the behaviour of the entire distribution at very small values: The expectation was that the model reproduces $\Gamma_t = 2.0\,\text{GeV}$ almost exactly for a vanishing value of σ_{det}, whereas the plot shows that the decay width tends to a value of 2.3 GeV.

5.8. Variation of the Prior Width of the Detector Resolution

This study simulates the variation of "knowledge" about the detector resolution. For this, the width of the Gaussian prior of σ_{det} was varied in a range of 0.0–2.0 GeV which included the default setting of an exactly known detector resolution, i.e. a prior width of 0.0 GeV. It is expected that the precision of the measurement of Γ_t decreases drastically with an increasing prior width. The corresponding plot is given in figure 5.10.

The plot shows that the uncertainty of Γ_t increases considerably from left to right beginning with a 68% interval of about 2 GeV and ending with about 17 GeV at the maximum prior width. An unexpected observation is the fact that both estimators tend to high values of Γ_t rising to values of over 10 GeV. Even if the uncertainty increases simultaneously, the initial value is excluded by the 68% interval at prior widths bigger

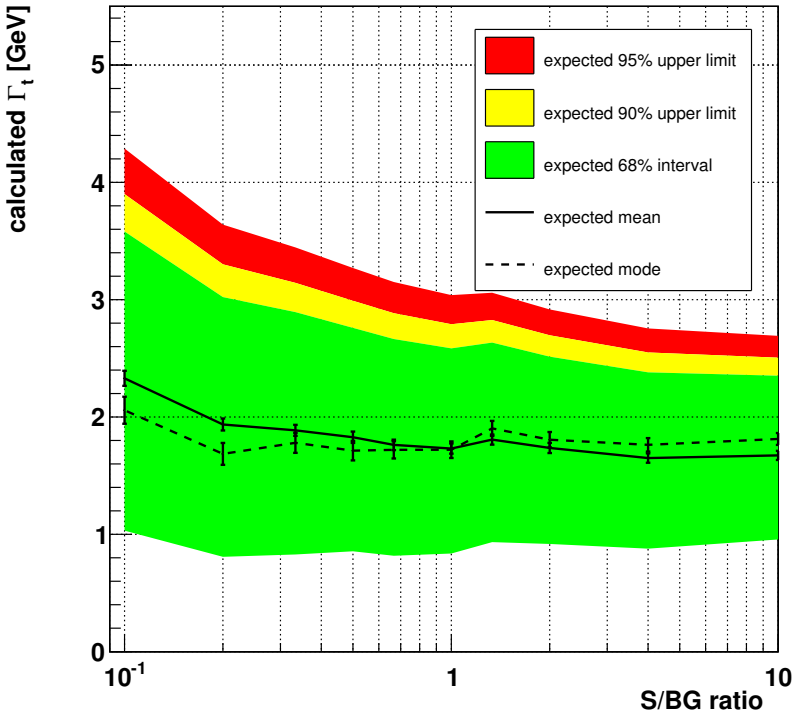

Figure 5.8.: Evaluation plot of the sensitivity study in which the S/BG ratio was varied.

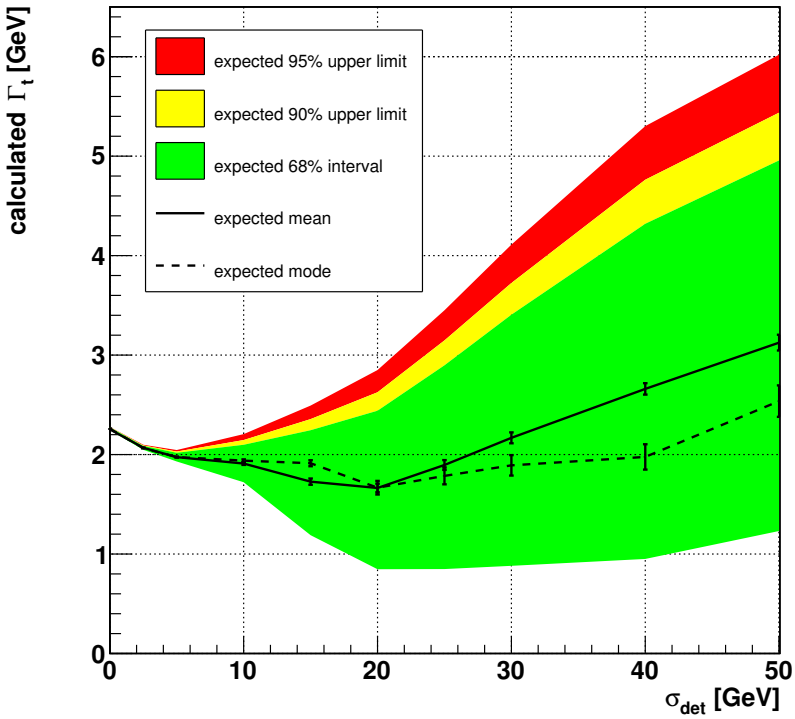

Figure 5.9.: Evaluation plot of the sensitivity study in which σ_{det} was varied.

than 0.6 GeV. Due to this strong bias of both estimators, the global mode, which takes all parameters into account for the determination of the "best" value, was marked as well.

One reason for this can be found in the figures 5.11 and 5.12. The first plot shows the knowledge update for the detector resolution in a run with a prior width of (only) 0.4 GeV. The posterior plot is strongly skewed and excludes almost half of the prior parameter range. This can be explained with the connection between Γ_t and σ_{det} over $\sqrt{\sigma_t^2 + \sigma_{\text{det}}^2}$ in eq. (4.11): Since Γ_t is limited to values above 0 GeV, the detector resolution cannot exceed 20 GeV because the square root is fixed by the data sample.

The strong link between both parameters can be seen in the correlation plot in the second figure 5.12. Due to the large statistics of $n_{\text{signal}} = 2.5 \cdot 10^6$ events the band of possible parameter combinations $(\Gamma_t \mid \sigma_{\text{det}})$ is very narrow. Since the parameters are strongly anti-correlated as well, the used MCMC algorithm fails to choose the best values for Γ_t and σ_{det} locally. However, the global mode is able to find the correct parameter set which corresponds to the initial values.

5.9. Variation of the Top Mass

To find out to what extent the assumption of a "wrong" top mass effects the results, the initial top mass, i.e. the one that was used for generating the pseudo-data, was varied; in the template fit the constant of $m_t = 172.5$ GeV was fixed. The top mass varied in the range 170–175 GeV, the step size was reduced to 0.1 GeV in the area of $m_t = 172.5$ GeV. The evaluation plot of the study can be found in figure 5.13.

The graph shows that the decay width is reproduced very reliably in the range of 172.5 GeV: Both estimators are almost at the initial value of 2.0 GeV and the 68% interval is distributed very evenly around this value. However, it is striking that the decay width is reproduced with a very high precision in the boundary regions, i.e. near 170 GeV and 175 GeV, but reproduced on an incorrect value. There is the general trend that with greater distance from the assumed value of 172.5 GeV, the precision increases further, while the calculated decay width moves away from the initial value more and more. Contrary to expectation, there is no axis of symmetry of the distribution around the assumed value of 172.5 GeV; the calculated decay width even keeps dropping to smaller values of m_t, so that around $m_t = 172.0$ GeV the initial value is no longer included in the 68% interval.

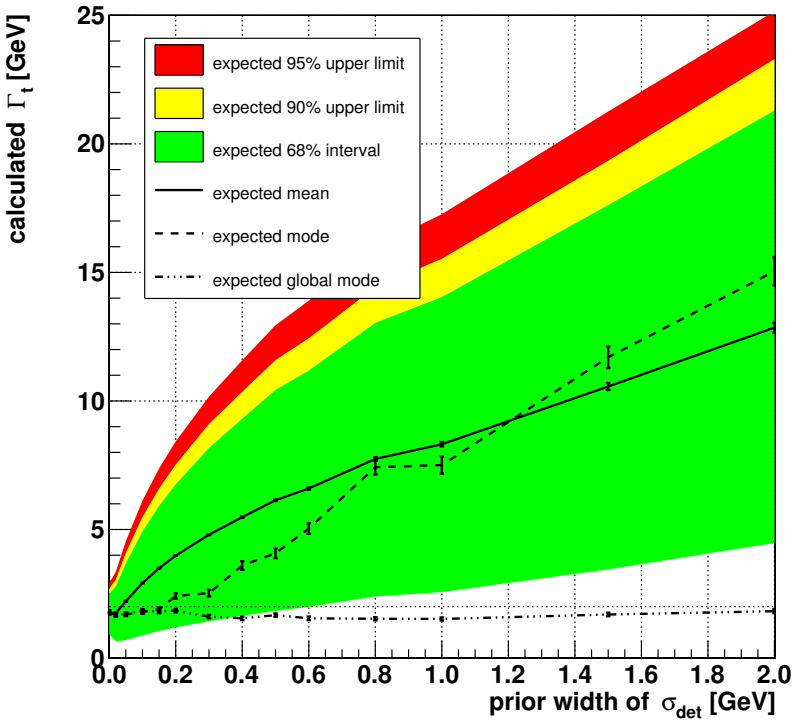

Figure 5.10.: Evaluation plot of the variation of the prior width of σ_{det}.

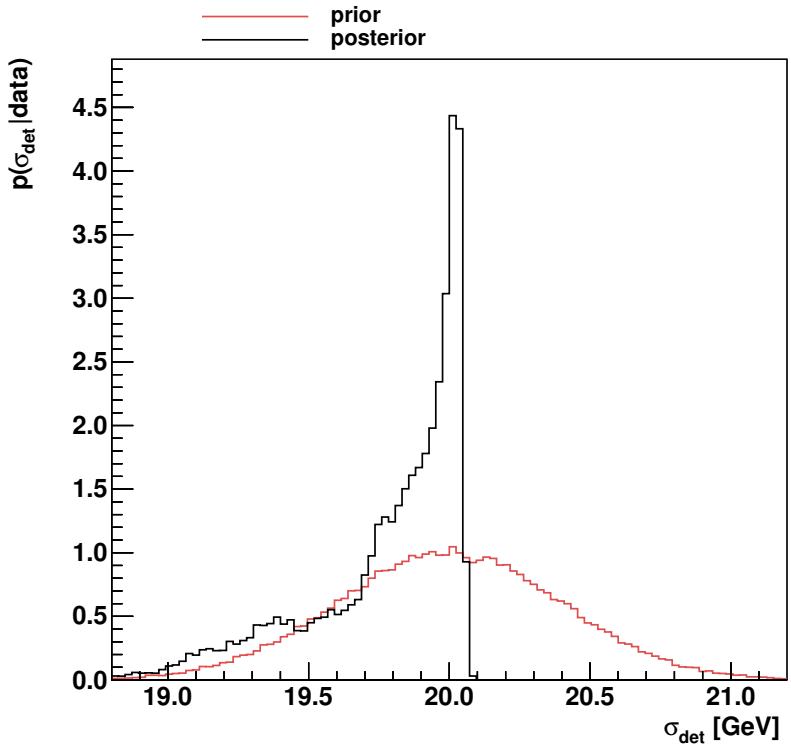

Figure 5.11.: Knowledge-update plot of a data sample with a prior width of 0.4 GeV.

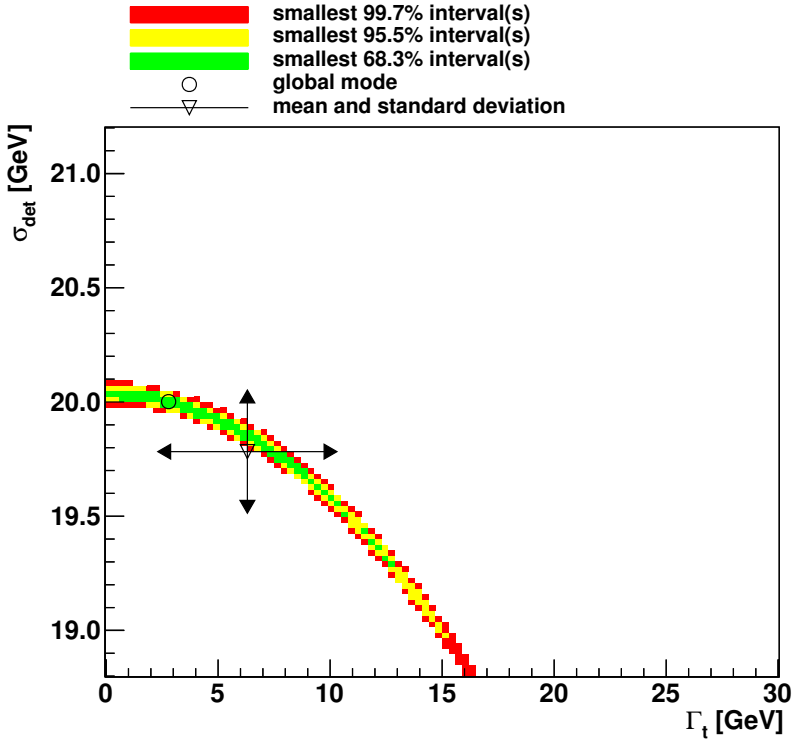

Figure 5.12.: Correlation plot between Γ_t and σ_{det} from a data sample with a prior width of the detector resolution of 0.4 GeV.

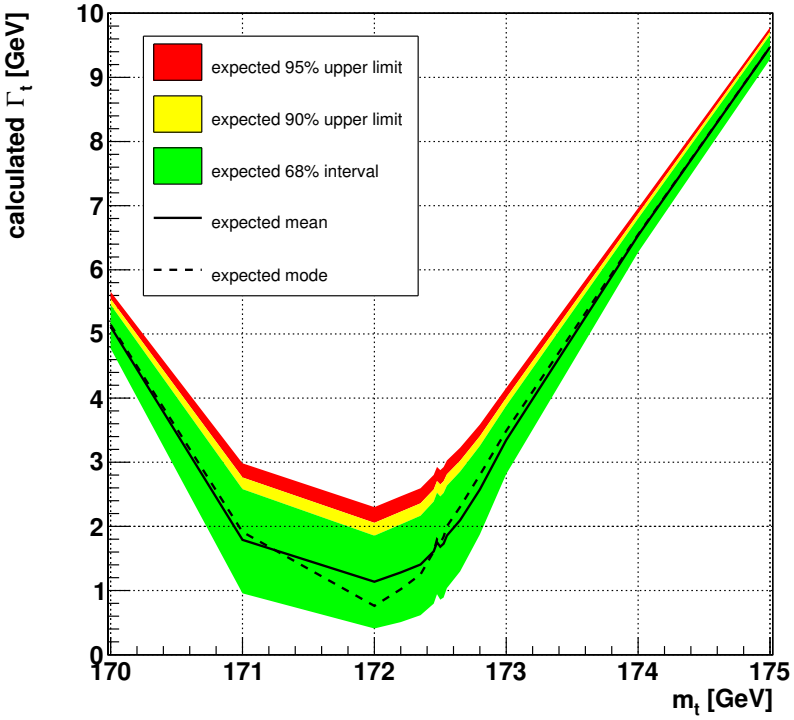

Figure 5.13.: Evaluation plot of the sensitivity study in which the input top mass was varied. In order to maintain the clarity, the data points as well as their error bars are not displayed.

6. Summary and Conclusions

In this thesis, the measurability of the top-quark decay width was examined. The investigation dealt with the question if a direct measurement of the decay width is possible at the LHC under the condition that all other influencing parameters are known precisely.

For this, simplified models were created by using pseudo-data samples in which the real situation of a top-quark-mass measurement was imitated. Chapter 4 started with a convolution of a Gaussian and a Breit-Wigner distribution and made a transition to a convolution of two Gaussian distributions. These models were calculated with the ML-fit approach and were done with the constraint that both the top-quark mass and the parameter describing the resolution of the detector were fixed. For both models, a set of 10,000 data samples was evaluated. The results showed that the fitted values and the input values of the top-quark decay width converged and therefore both models were able to reproduce the decay width correctly.

In chapter 5, sensitivity studies were done to test out to what extent the different model parameters affect the results. For these studies, the model was expanded by introducing a simulation of background events and by using a template-fit approach. For the calculations, prior probability densities for σ_{det} were considered to simulate a certain degree of uncertainty on the value.

First of all, the sensitivity studies showed that a reconstruction of the decay width is possible indeed, but is highly dependent on the model parameters. The corresponding sensitivity study yielded that the bin width d has to be significantly smaller than the quantity to be measured to prevent the model from a strong bias. A variation of the input value of Γ_t led to the conclusion that the two used estimators "mean" and "mode" are both biased when the input value is set to small values below 2 GeV. Nonetheless, the model is able to reproduce the input decay width with high accuracy for values above this threshold.

A variation of the statistics showed that the degree of determination of the decay width is strongly connected with the size of the data sample, i.e. the number of events. The precision of the estimators increases a lot with large numbers of events while the expected

uncertainties decrease. To make a very rough estimate, there are expected to be about 100,000 $t\bar{t}$ events in the full data set of $5\,\mathrm{fb}^{-1}$ at $\sqrt{s} = 7\,\mathrm{TeV}$ and $21\,\mathrm{fb}^{-1}$ at $\sqrt{s} = 8\,\mathrm{TeV}$ at the LHC after event selection. According to the study, it will be possible to obtain precisely measured values of the top-quark decay width with this amount of data. Additionally, another study showed that the ratio of signal and background events must only be roughly around the value of 1:1 and has no big influence on the precision of the measurement.

The studies on the variation of the detector resolution and the prior width of the detector resolution showed that this parameter strongly influences the accuracy of the measurement as well. The more the detector resolution is reduced, the more accurate is the obtained value of the decay width. A vague value of the detector resolution (even at small values of the prior width) leads to a significant bias in the measurement and the reconstructed value and the input value diverge quickly. As a conclusion, it will be one of the main challenges for future measurements of the decay width to get to know and understand the energy resolution of the detector (especially the JES) as good as possible in order to allow precise measurements.

The last study showed that an incorrectly assumed value of the top-quark mass also causes a strong bias in the reconstruction. This leads as well to the conclusion that the JES has to be quantified very accurately to make an unbiased measurement possible. At this point, the model could be extended by considering the different effects leading to the uncertainty of the mass reconstruction. In a more complex form, they could be parameterized in the detector resolution function.

A. Other figures and graphics

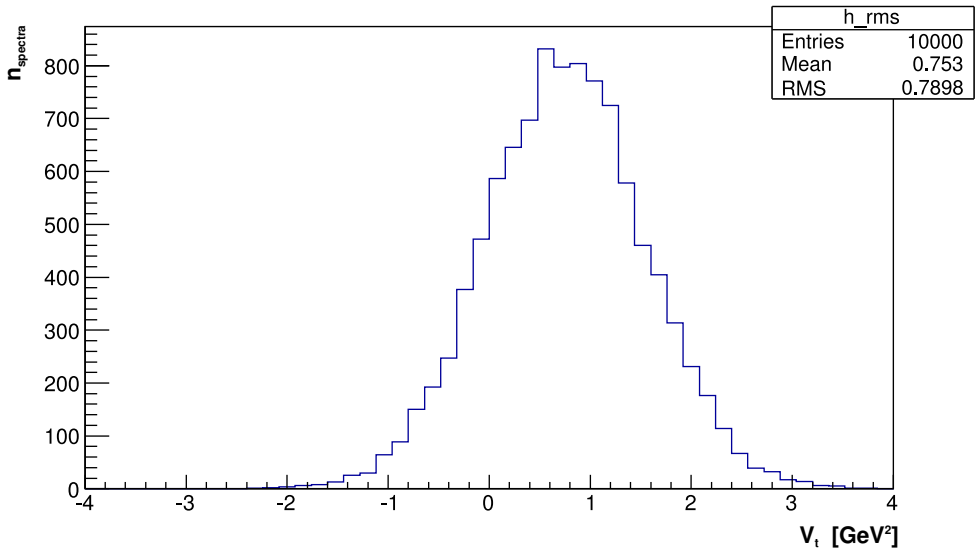

(a) The fitted values for the variance V_t

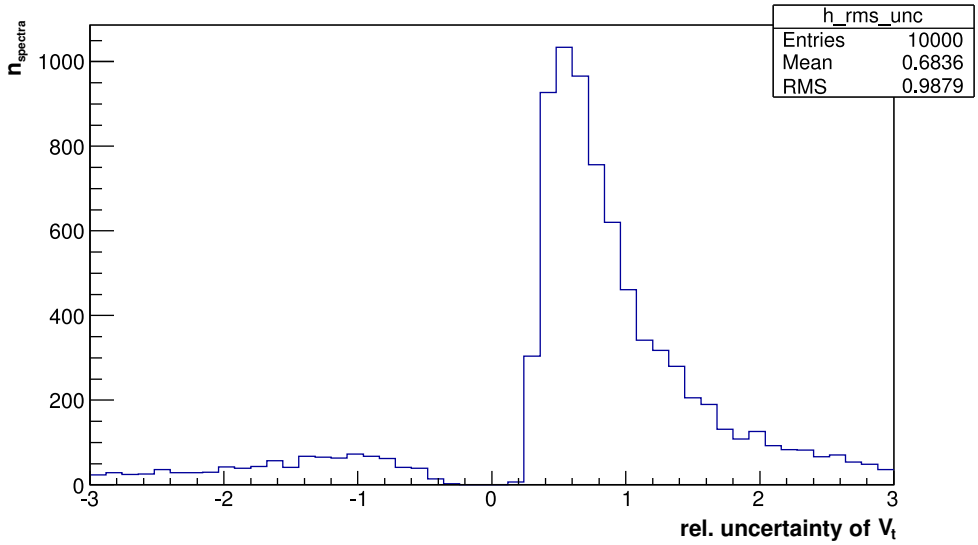

(b) The corresponding relative uncertainties

Figure A.1.: Results of the convolution of two Gaussian distributions with the use of their variances.

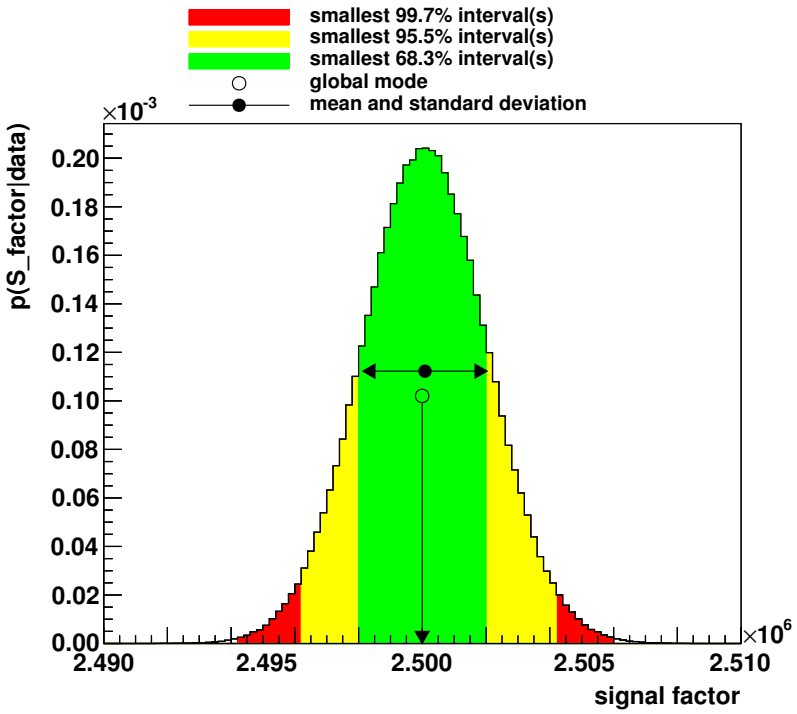

Figure A.2.: Example of a marginalized distribution of the signal factor for the default parameter setting (see section 5.1).

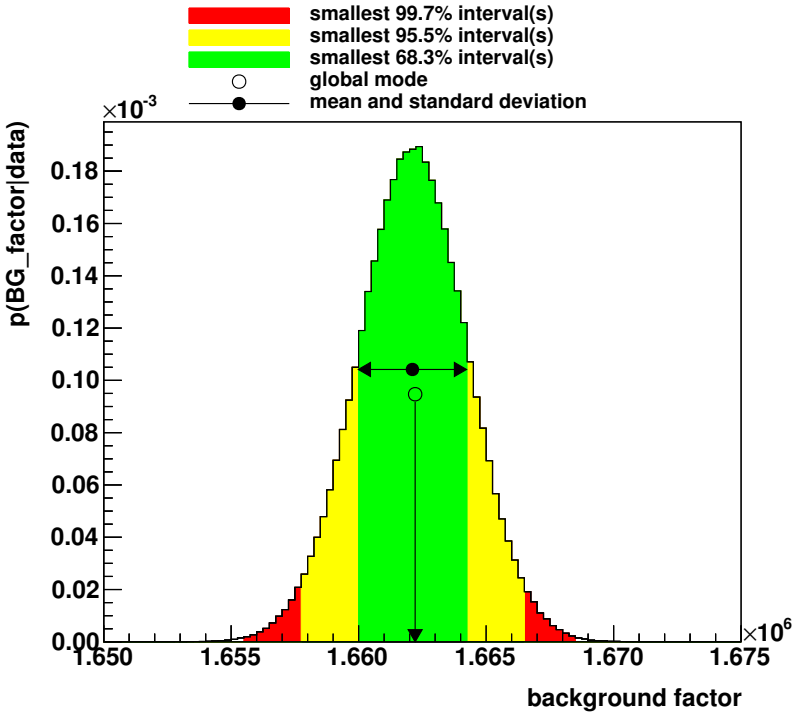

Figure A.3.: Example of a marginalized distribution of the background factor for the default parameter setting (see section 5.1).

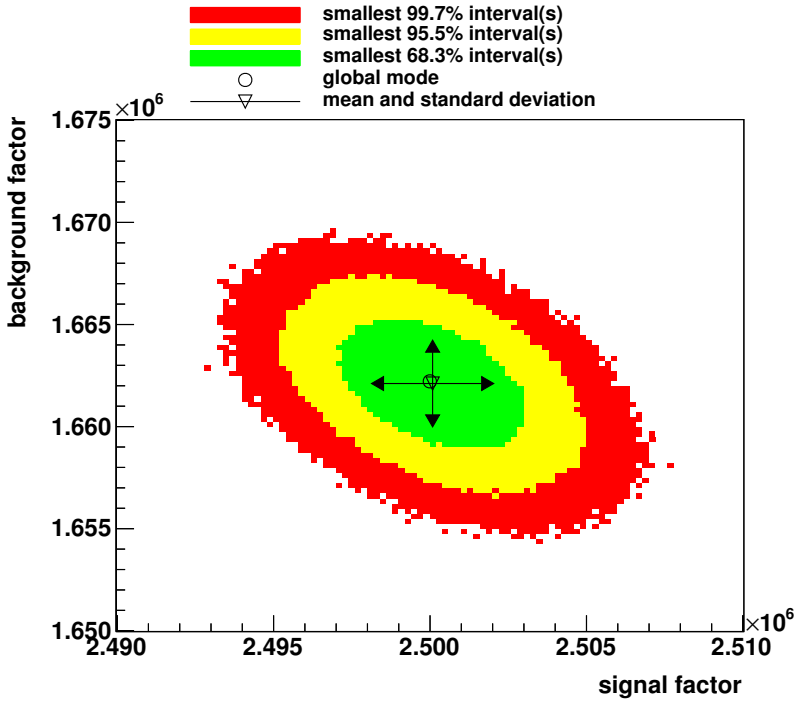

Figure A.4.: Example of a correlation plot of the signal and the background factor. For this, the default parameter setting was used (see section 5.1).

Bibliography

[1] G. Aad, et al. (ATLAS Coll.), *Observation of a new particle in the search for the Standard Model Higgs boson with the ATLAS detector at the LHC*, Phys. Lett. B **716(1)**, 1 (2012)

[2] S. Chatrchyan, et al. (CMS Coll.), *Observation of a new boson at a mass of 125 GeV with the CMS experiment at the LHC*, Phys. Lett. B **716(1)**, 30 (2012)

[3] P. W. Higgs, *Broken Symmetries, Massless Particles and Gauge Fields*, Phys. Lett. **12**, 132 (1964)

[4] F. Englert, R. Brout, *Broken Symmetry and the Mass of Gauge Vector Mesons*, Phys. Rev. Lett. **13**, 321 (1964)

[5] F. Abe, et al. (CDF Coll.), *Observation of Top Quark Production in $p\bar{p}$ Collisions with the Collider Detector at Fermilab*, Phys. Rev. Lett. **74**, 2626 (1995)

[6] S. Abachi, et al. (DØ Coll.), *Observation of the Top Quark*, Phys. Rev. Lett. **74**, 2632 (1995)

[7] D. J. Griffiths, *Introduction to Elementary Particles*, Wiley-VCH, 2nd, revised edition (2008)

[8] MissMJ, wikipedia.org (publisher), *File:Standard Model of Elementary Particles.svg*, [Retrieved: January 23, 2014, 18:39], URL `http://en.wikipedia.org/wiki/File:Standard_Model_of_Elementary_Particles.svg`

[9] J. Beringer, et al. (Particle Data Group), *Review of Particle Physics*, Phys. Rev. D **86**, 010001 (2012)

[10] M. Gell-Mann, *The interpretation of the new particles as displaced charge multiplets*, Il Nuovo Cimento **4(2)**, 848 (1956)

[11] T. Nakano, K. Nishijima, *Charge Independence for V-particles*, Prog. Theor. Phys. **10(5)**, 581 (1953)

[12] M. Gell-Mann, *A schematic model of baryons and mesons*, Phys. Lett. **8(3)**, 214 (1964)

[13] G. Zweig, *An SU_3 model for strong interaction symmetry and its breaking*, CERN-TH-401 (1964, unpublished)

[14] Y. Fukuda, et al. (Super-Kamiokande Coll.), *Evidence for Oscillation of Atmospheric Neutrinos*, Phys. Rev. Lett. **81**, 1562 (1998)

[15] Q. R. Ahmad, et al. (SNO Coll.), *Measurement of the Rate of $\nu + d \rightarrow p + p + e^-$ Interactions Produced by ^8B Solar Neutrinos at the Sudbury Neutrino Observatory*, Phys. Rev. Lett. **87**, 071301 (2001)

[16] K. Eguchi, et al. (KamLAND Coll.), *First Results from KamLAND: Evidence for Reactor Antineutrino Disappearance*, Phys. Rev. Lett. **90**, 021802 (2003)

[17] G. S. Guralnik, C. R. Hagen, T. W. B. Kibble, *Global Conservation Laws and Massless Particles*, Phys. Rev. Lett. **13**, 585 (1964)

[18] W. Heisenberg, *Über den anschaulichen Inhalt der quantentheoretischen Kinematik und Mechanik*, Zeitschrift für Physik **43(3-4)**, 172 (1927)

[19] E. Kennard, *Zur Quantenmechanik einfacher Bewegungstypen*, Zeitschrift für Physik **44(4-5)**, 326 (1927)

[20] C. S. Wu, et al., *Experimental Test of Parity Conservation in Beta Decay*, Phys. Rev. **105**, 1413 (1957)

[21] J. H. Christenson, et al., *Evidence for the 2π Decay of the K_2^0 Meson*, Phys. Rev. Lett. **13**, 138 (1964)

[22] N. Cabbibo, *Unitary Symmetry and Leptonic Decays*, Phys. Rev. Lett. **10**, 531 (1963)

[23] S. L. Glashow, J. Iliopoulos, L. Maiani, *Weak Interactions with Lepton-Hadron Symmetry*, Phys. Rev. D **2**, 1285 (1970)

[24] M. Kobayashi, T. Maskawa, *CP Violation in the Renormalizable Theory of Weak Interaction*, Prog. Theor. Phys. **49**, 652 (1973)

[25] T. Aaltonen, et al. (CDF & DØ Coll.), *Combination of the top-quark mass measurements from the Tevatron collider*, Phys. Rev. D **86**, 092003 (2012)

[26] ATLAS Coll., *Combination of ATLAS and CMS results on the mass of the top-quark using up to 4.9 fb^{-1} of $\sqrt{s}$ = 7 TeV LHC data*, ATLAS-CONF-2013-102 (2013, unpublished)

[27] M. Jeżabek, J. H. Kühn, *QCD Corrections to Semileptonic Decays of Heavy Quarks*, Nucl. Phys. B **314**, 1 (1989)

[28] V. M. Abazov, et al. (DØ Coll.), *Improved determination of the width of the top quark*, Phys. Rev. D **85**, 091104 (2012)

[29] T. Aaltonen, et al. (CDF Coll.), *Direct Measurement of the Total Decay Width of the Top Quark*, Phys. Rev. Lett. **111**, 202001 (2013)

[30] CDF Coll., *A Direct Top Quark Width Measurement at CDF*, CDF note 10936 (2012, unpublished)

[31] I. I. Y. Bigi, et al., *Production and decay properties of ultraheavy quarks*, Phys. Lett. B **181**, 157 (1986)

[32] L. H. Orr, J. L. Rosner, *Comparison of top quark hadronization and decay rates*, Phys. Lett. B **246**, 221 (1990)

[33] V. M. Abazov, et al. (DØ Coll.), *Observation of Single Top-Quark Production*, Phys. Rev. Lett. **103**, 092001 (2009)

[34] T. Aaltonen, et al. (CDF Coll.), *Observation of Electroweak Single Top-Quark Production*, Phys. Rev. Lett. **103**, 092002 (2009)

[35] G. Aad, et al. (ATLAS Coll.), *Measurement of the top quark pair cross section with ATLAS in pp collisions at $\sqrt{s}$ = 7 TeV using final states with an electron or a muon and a hadronically decaying τ lepton*, Phys. Lett. B **717(1-3)**, 89 (2012)

[36] G. Aad, et al. (ATLAS Coll.), *Measurement of the t-channel single top-quark production cross section in pp collisions at $\sqrt{s}$ = 7 TeV with the ATLAS detector*, Phys. Lett. B **717(4-5)**, 330 (2012)

[37] T. Aaltonen, et al. (CDF and DØ Coll.), *Combination of measurements of the top-quark pair production cross section from the Tevatron Collider*, FERMILAB-PUB-13-432-E (2013, unpublished)

[38] DØ Coll., *Feynman Diagrams for Top Physics Talks and Notes*, [Retrieved: January 20, 2014, 17:19], URL `http://www-d0.fnal.gov/Run2Physics/top/top_public_web_pages/top_feynman_diagrams.html`

[39] Atlas Coll., *Determination of the Top Quark Mass with a Template Method in the All-Hadronic Decay Channel using 2.04 fb^{-1} of ATLAS Data*, ATLAS-CONF-2012-030 (2012, unpublished)

[40] Atlas Coll., *Luminosity Public Results*, [Retrieved: January 24, 2014, 13:37], URL `https://twiki.cern.ch/twiki/bin/view/AtlasPublic/LuminosityPublicResults`

[41] Atlas Coll., *ATLAS Detector and Physics Performance TDR, Volume I+II*, CERN/LHCC 99-14/15 (1999, unpublished)

[42] Atlas Coll., *ATLAS Experiment – Photos*, [Retrieved: January 10, 2014, 11:01], URL `http://www.atlas.ch/photos/full-detector-cgi.html`

[43] G. Cowan, *Statistical Data Analysis*, Oxford University Press (1998)

[44] I. Bronstein, et al., *Taschenbuch der Mathematik*, Harri Deutsch, 7th, revised edition (2008)

[45] R. J. Barlow, *Statistics*, John Wiley & Sons (1999)

[46] G. Aad, et al. (Atlas Coll.), *Measurement of the top quark mass with the template method in the $t\bar{t} \to \text{lepton} + \text{jets}$ channel using ATLAS data*, Eur. Phys. J. C **72(6)**, 1 (2012)

Acknowledgements

First of all, I would like to thank Prof. Dr. Arnulf Quadt for being my referee as well as my group leader who gave me the opportunity to be a part of his working group and to write this thesis there. Second, I would also like to thank the second referee, Prof. Dr. Ariane Frey. Especially her appealing lectures inspired me to write my Bachelor's thesis on the topic of particle physics.

For his constant effort to help me, I would like to express my thanks to my supervisor for this thesis, Priv.-Doz. Dr. Kevin Kröninger. He was always available for discussions about my work and he always had sympathetic ears for my numerous questions.

Erklärung nach §13(8) der Prüfungsordnung für den Bachelor-Studiengang Physik und den Master-Studiengang Physik an der Universität Göttingen:

Hiermit erkläre ich, dass ich diese Abschlussarbeit selbständig verfasst habe, keine anderen als die angegebenen Quellen und Hilfsmittel benutzt habe und alle Stellen, die wörtlich oder sinngemäß aus veröffentlichten Schriften entnommen wurden, als solche kenntlich gemacht habe.
Darüberhinaus erkläre ich, dass diese Abschlussarbeit nicht, auch nicht auszugsweise, im Rahmen einer nichtbestandenen Prüfung an dieser oder einer anderen Hochschule eingereicht wurde.

Göttingen, den 27. Januar 2014

(Knut Zoch)